INSTITUT FÜR INFORMATIK

The 2D Analytic Signal

Lennart Wietzke and Gerald Sommer

Bericht Nr. 0802
September 1, 2008

CHRISTIAN-ALBRECHTS-UNIVERSITÄT
ZU KIEL

Institut für Informatik der
Christian-Albrechts-Universität zu Kiel
Olshausenstr. 40
D – 24098 Kiel

The 2D Analytic Signal

Lennart Wietzke and Gerald Sommer

Bericht Nr. 0802
September 1, 2008

e-mail: lw@ks.informatik.uni-kiel.de

Abstract

Keywords: Isotropic, phase based, local signal analysis, analytic signal, monogenic signal, conformal space, projective space, Hilbert transform, Radon transform, Clifford analysis, hybrid matrix geometric algebra.

This technical report covers a fundamental problem of 2D *local phase based* signal processing: the isotropic generalization of the *analytic signal* (D. Gabor) for two dimensional signals. The *analytic signal* extends a *real valued* 1D signal to a *complex valued* signal by means of the classical 1D Hilbert transform. This enables the complete analysis of local phase and amplitude information. Local phase, amplitude and additional orientation information can be extracted by the *monogenic signal* (M. Felsberg and G. Sommer) which is always restricted to the subclass of *intrinsically one dimensional signals*. In case of 2D image signals the monogenic signal enables the rotationally invariant analysis of lines and edges. In contrast to the 1D analytic signal the *monogenic signal* extends all *real valued* signals of dimension n to a $(n + 1)$ - dimensional *vector valued* monogenic signal by means of the generalized first order Hilbert transform (Riesz transform). In this technical report we present the *2D analytic signal* as a novel generalization of the 2D *monogenic signal* which now extends the original 2D signal to a *multivector valued* signal in *conformal space* by means of higher order Hilbert transforms and by means of a *hybrid matrix geometric algebra* representation. The 2D analytic signal can be interpreted in conformal space which delivers a descriptive geometric interpretation of 2D signals. One of the main results of this work is, that all 2D signals exist per se in a 3D projective subspace of the conformal space and can be analyzed by means of geometric algebra. In case of 2D image signals the 2D analytic signal enables now the rotational invariant analysis of lines, edges, corners and junctions.

Contents

Chapter 1

Introduction

Low level two-dimensional image analysis is often the first step of many computer vision tasks. Therefore, local signal features with geometrical and structural information determine the quality of subsequent higher level processing steps. It is important not to lose or to merge any of the original signal information within the local neighborhood of the test point[1]. The constraints of local signal analysis are: to span an orthogonal feature space (split of identity) and to be robust against stochastic and deterministic deviations between the actual signal and the assumed signal model.
One of the fundamental problems in signal processing is a good signal representation. Such a signal representation is the local phase information which is a robust feature with respect to noise transformations [20, 14, 13]. In case of image signals it is shown in [24] that the original signal can be recovered to a fairly large extend by using only its phase information while setting its amplitude information to unity. In contrast to that, if only the amplitudes are obtained and the phases are set to zero, the recovered image signal is completely indiscernible. Therefore phase based signal processing has found success in many applications, such as disparity estimation of stereo [14], matching [6], face recognition [29], etc.
This technical report is organized as follows: First a 1D signal model and the related classical analytic signal will be introduced which extends the 1D real valued signal to a complex valued one by means of the classical Hilbert transform. It will be shown that the assumed signal model results from the application of a scale space operator to the original signal.
To solve problems of 2D signal processing, first 2D signals will be classified

[1]There is no method of signal analysis which is universal in respect of any arbitrary local 2D structure. Hence, it is necessary to formulate a model of local signal structure as basis of the analysis. The great challenge is the search for a most general model which can cope with as much as possible variants of local signal structure.

into classes of different intrinsic dimensions.
Furthermore, to extend the analytic signal the classical 1D Hilbert transform will be generalized to the so called Riesz transform of arbitrary order, abbreviated by Hilbert transform. In this context the relation of the 2D Hilbert transform and the 2D Radon transform will be shown which is essential for interpretation of the assumed signal models.
Since the signal models result from the application of the Poisson scale space operator to the original signal, the Hilbert transforms of order one, two and three will be derived in Poisson scale space.
By means of the first order Hilbert transform now signals of intrinsic dimension one (i1D) can be analyzed by the 2D monogenic signal. The interpretation of the 2D monogenic signal as a 3D vector in Euclidean space will be done geometrically.
To get rid of the restriction to i1D signals now also i1D and i2D signal models will be defined and analyzed by the first order and second order Hilbert transform. It will be shown that real valued 2D signals may be written in matrix form which are isomorphic to so called multivectors in conformal space by means of a hybrid matrix geometric algebra. The result of this mapping is that 2D signals exist per se in a 3D projective subspace of the conformal space which can be used for analyzing 2D signals and separation of superimposed i1D signals which build up the 2D signals.
In the practical part of this report the 2D analytic signal will be implemented in C++, discussed and some results of the 2D analytic signal will be illustrated as well as some quantitative experimental 3D plots will be presented with comparisons of the 2D monogenic signal and the 2D analytic signal.
In the final outlook a generalization of the 2D analytic signal to any signal model will be constructed. The goal of future work will therefore be the general geometric interpretation of 2D signals in conformal space.

Chapter 2

The 1D Analytic Signal

To solve phase based 2D signal analysis problems, first phase based 1D signal analysis has to be considered. From Fourier analysis it is well known that each 1D signal $g \in L_2(\mathbb{R}, \mathbb{R})$ can be approximated with infinite small error by its Fourier series

$$g(x) = \sum_{\nu} a_\nu \cos(2\pi\nu x + \phi_\nu)$$

with ν as the frequency. Each frequency component with its appropriated individual phase and amplitude can be analyzed separately. This selected frequency of interest carries the structural information of the signal and has to be extracted from the original signal by applying a filter operator $\mathcal{P}\{\cdot\}$ before analysis. Therefore, the local 1D signal model at the origin 0 of the applied local coordinate system reads

$$g^e := a \cos\phi := a_s \cos\phi_s = \mathcal{P}\{g\}(0; s)$$

with the abbreviation $a := a_s$, $\phi := \phi_s$ and with $s > 0$ as the scale space parameter of the filter operator $\mathcal{P}\{\cdot\}$ which will be specified later. Since the local signal model is assumed to be an even function (i.e. $\cos(x) = \cos(-x)\ \forall x \in \mathbb{R}$) it is called the *even part* g^e of the *analytic signal.* The corresponding *odd part* can be calculated by means of convolution of the filtered original signal with the classical 1D Hilbert transform kernel $h(\tau) := \frac{1}{\pi\tau}$

$$g^o := a \sin\phi := a_s \sin\phi_s = (h * \mathcal{P}\{g\})(0; s)$$

with $*$ as the 1D convolution operator and

$$(h * \mathcal{P}\{g\})(x; s) = \frac{1}{\pi}\text{P.V.}\int_{\tau\in\mathbb{R}} \frac{\mathcal{P}\{g\}(x-\tau; s)}{\tau} d\tau$$

as the classical 1D Hilbert transform of the signal g in scale space and P.V. as the Cauchy principal value. Since the Hilbert transform of the original signal is locally an odd function (i.e. $\sin(x) = -\sin(-x)\ \forall x \in \mathbb{R}$) it is called the *odd part* g^o of the analytic signal.
One important local structural feature of the filtered signal $\mathcal{P}\{g\}$ is the local phase $\phi \in [0, 2\pi)$ [22] because it is independent of the local signal amplitude a [18]. The local phase can be determined by

$$\phi = \arctan \frac{g^o}{g^e}$$

and the local signal amplitude can be determined by

$$a = \sqrt{[g^e]^2 + [g^o]^2}\ .$$

The vector valued extension $[g^e, g^o]^T$ of a scalar valued one-dimensional signal g is called *analytic signal*. Note that originally the analytic signal has been defined as a complex valued signal with g^e as the real part and g^o as the imaginary part [16].
The 1D analytic signal has been used also in 2D signal processing. This makes necessary to extend the classical 1D Hilbert transform to multiple dimensions. There are several approaches in the literature which lack the required rotational invariance of the multidimensional Hilbert transform, see [19, 5].
One possible generalization of the one-dimensional Hilbert transform to higher dimensions is the Riesz transform which will be called Hilbert transform in this technical report.

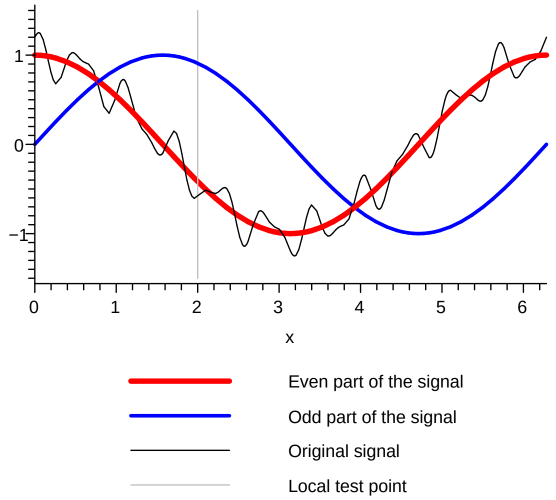

Figure 2.1: Illustration of a 1D signal and its even and odd part in scale space (for the frequency $\nu = 1\text{Hz}$) with local amplitude $a = 1$ and local phase $\phi = 2$ at the test point $x = 2$ of local interest.

Chapter 3

2D Signal Classification

2D signals $f \in L_2 := L_2(\mathbb{R}^2, \mathbb{R})$ are classified into local regions $N \subseteq \Omega$ of different intrinsic dimensions [31] (which correspond to their codimension). The intrinsic dimension expresses the number of degrees of freedom necessary to describe local structure. Constant signals are of intrinsic dimension zero (i0D), lines and edges are of intrinsic dimension one (i1D) and all other possible patterns are of intrinsic dimension two (i2D) (see figure 3.1)

$$\begin{aligned}
\text{i0D} &:= \{f \in L_2 : f(\mathbf{x}_i) = f(\mathbf{x}_j)\ \forall \mathbf{x}_i, \mathbf{x}_j \in N\} \\
\text{i1D} &:= \{f \in L_2 : f(x,y) = g(x\cos\theta + y\sin\theta)\ \forall (x,y) \in N\} \setminus \text{i0D} \\
\text{i2D} &:= L_2 \setminus (\text{i0D} \cup \text{i1D})
\end{aligned}$$

with $g \in L_2(\mathbb{R}, \mathbb{R})$. In general i2D signals can only be modeled by an infinite number of superimposed i1D signals. Therefore, it is essential to assume a certain signal model or a set of certain models for exact i2D signal analysis. Furthermore the intrinsic dimension depends also on the *scale* at which the signal will be considered locally.
From a statistically point of view, the frequency of occurrence of local regions with different intrinsic dimension in real 2D images appears in the following upward order

$$\begin{aligned}
& \left\| \bigcup_j \{(x,y) \in N_j : f|_{N_j} \in \text{i0D}\} \right\| \\
> & \left\| \bigcup_j \{(x,y) \in N_j : f|_{N_j} \in \text{i1D}\} \right\| \\
> & \left\| \bigcup_j \{(x,y) \in N_j : f|_{N_j} \in \text{i2D}\} \right\|
\end{aligned}$$

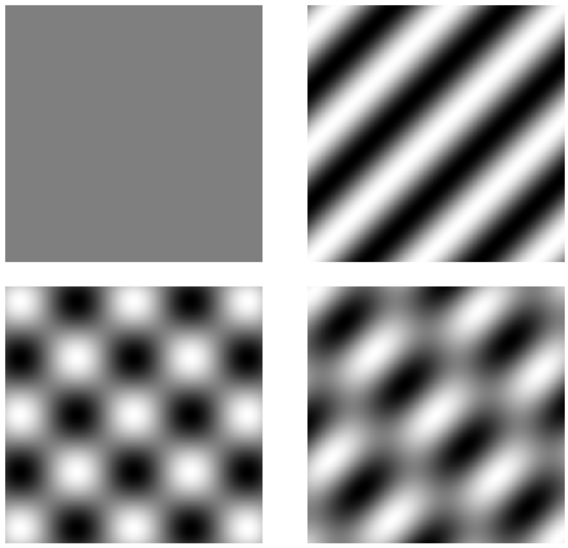

Figure 3.1: Top row from left to right: A constant signal (i0D) and an arbitrarily rotated 1D signal (i1D). Bottom row from left to right: Two i2D signals which consist of two superposed i1D signals. Note that all signals displayed here preserve their intrinsic dimension globally.

with the partition $\Omega = \dot{\bigcup}_j N_j$ of the image signal.

Chapter 4

Generalized Hilbert Transform

Phase based [6] 1D signal analysis will be done by the analytic signal and the classical 1D Hilbert transform [16]. Analysis of 2D signals will be done by the generalized Hilbert transform [4] which will be abbreviated by Hilbert transform. The Hilbert transform is also known as Riesz transform. To enable *local* signal analysis in scale space with individual scale space parameters at every test point within the 2D signal, it is essential that the Hilbert transform of arbitrary order n can be done by convolution in spatial domain and without the need of Fourier transformation.
Instead of writing the spatial domain coordinates in vector form $(x, y) \in \mathbb{R}^2$, they will be now expressed as a complex number $z \in \mathbb{C}$ with $z := x + \mathbf{i}y$. According to [21] for $\xi := \xi_1 + \mathbf{i}\xi_2 \in \mathbb{C}$ and the 2D signal $f \in L_2(\mathbb{C}, \mathbb{R})$ the Hilbert transform of order $n \in \mathbb{N}$ is defined by

$$\begin{aligned} \mathcal{H}^{(n)}\{f\}(z) &:= \underbrace{\mathcal{H}\{\mathcal{H}\{\ldots\mathcal{H}\{f\}\}\}}_{n\text{-times}}(z) \\ &= -\frac{n}{2\pi}\int\limits_{\xi\in\mathbb{C}} \frac{f(\xi)}{(z-\xi)^n\|z-\xi\|^{2-n}}\,d\xi\ . \end{aligned}$$

4.1 First Order Hilbert Transform

For $n = 1$ the ordinary first order Hilbert transform in two dimensions is obtained as

$$\begin{aligned}
\mathcal{H}^{(1)}\{f\}(z) &= -\frac{1}{2\pi} \int\limits_{\xi \in \mathbb{C}} \frac{f(\xi)}{(z-\xi)\|z-\xi\|}\, d\xi \\
&= -\frac{1}{2\pi} \int\limits_{\xi \in \mathbb{C}} \frac{(x-\xi_1)}{\|z-\xi\|^3} f(\xi)\, d\xi \\
&+ \mathbf{i}\frac{1}{2\pi} \int\limits_{\xi \in \mathbb{C}} \frac{(y-\xi_2)}{\|z-\xi\|^3} f(\xi)\, d\xi \\
&= -\mathcal{H}_x\{f\}(z) + \mathbf{i}\mathcal{H}_y\{f\}(z)\ .
\end{aligned}$$

This results in the following 2D convolution kernels of the first order Hilbert transform

$$h^{(1)}(x,y) = \begin{bmatrix} h_x \\ h_y \end{bmatrix}(x,y) = \frac{1}{2\pi(x^2+y^2)^{\frac{3}{2}}} \begin{bmatrix} x \\ y \end{bmatrix}$$

These kernels can be directly used to calculate the first order Hilbert transform of a two-dimensional signal $f \in L_2(\mathbb{R}^2, \mathbb{R})$ in spatial domain without the need of any Fourier transform.

4.2 Second Order Hilbert Transform

The convolution kernel in spatial domain of the second order Hilbert transform for ($n = 2$) results in the Beurling-Ahlfors transform for the signal $f \in L_2(\mathbb{C}, \mathbb{R})$ (which is without loss of generality defined on the complex numbers) and reads

$$
\begin{aligned}
& \mathcal{H}^{(2)}\{f\}(z) = -\frac{1}{\pi} \int\limits_{\xi\in\mathbb{C}} \frac{f(\xi)}{(z-\xi)^2}\, d\xi \\
= & -\frac{1}{\pi} \int\limits_{\xi\in\mathbb{C}} \frac{(x-\xi_1)^2 f(\xi)}{[(x-\xi_1)^2-(y-\xi_2)]^2+4(x-\xi_1)^2(y-\xi_2)^2}\, d\xi \\
+ & \frac{1}{\pi} \int\limits_{\xi\in\mathbb{C}} \frac{(y-\xi_2)^2 f(\xi)}{[(x-\xi_1)^2-(y-\xi_2)]^2+4(x-\xi_1)^2(y-\xi_2)^2}\, d\xi \\
+ & \mathbf{i}\frac{2}{\pi} \int\limits_{\xi\in\mathbb{C}} \frac{(x-\xi_1)(y-\xi_2) f(\xi)}{[(x-\xi_1)^2-(y-\xi_2)]^2+4(x-\xi_1)^2(y-\xi_2)^2}\, d\xi \\
= & -\mathcal{H}_{xx}\{f\}(z) + \mathcal{H}_{yy}\{f\}(z) + \mathbf{i}2\mathcal{H}_{xy}\{f\}(z)\ .
\end{aligned}
$$

This results in the following 2D convolution kernels of the second order Hilbert transform

$$
h^{(2)}(x,y) = \begin{bmatrix} h_{xx} \\ h_{xy} \\ h_{yy} \end{bmatrix}(x,y) = \frac{1}{\pi(x^2+y^2)^2} \begin{bmatrix} x^2 \\ xy \\ y^2 \end{bmatrix}\ .
$$

These kernels can be directly used to calculate the second order Hilbert transform of a two-dimensional signal $f \in L_2(\mathbb{R}^2, \mathbb{R})$ in spatial domain without the need of any Fourier transform.

4.3 Relation of the Hilbert Transform and the Radon Transform

The Hilbert transform can be expressed using the Radon transform, its inverse and the classical 1D Hilbert transform. Note that the relation to the Radon transform is required solely for interpretation and theoretical results. Neither the Radon transform nor its inverse are ever applied to the signal in practice. Instead, the Hilbert transformed signal will be determined by convolution with the Hilbert kernels in spatial domain. The 2D Radon transform $f_r(t,\theta) := \mathcal{R}\{f\}(t,\theta)$ [2] is defined by

$$
\mathcal{R}\{f\}(t,\theta) := \int\limits_{(x,y)\in\mathbb{R}^2} f(x,y)\ \delta_0(x\cos\theta + y\sin\theta - t)\ d(x,y)
$$

with $\theta \in [0, \pi)$ as the orientation, $t \in \mathbb{R}$ as the minimal distance of the line to the origin $(0,0) \in \mathbb{R}^2$ of the local coordinate system and δ_0 as the Dirac delta distribution. The inverse 2D Radon transform exists and is defined by

$$\mathcal{R}^{-1}\{f_r\}(x,y) := \frac{1}{2\pi^2} \int\limits_{\theta=0}^{\pi} \text{P.V.} \int\limits_{t\in\mathbb{R}} \frac{\frac{\partial}{\partial t} f_r(t,\theta)}{x\cos\theta + y\sin\theta - t}\, dt\, d\theta$$

Now the Hilbert transform will be expressed by the classical 1D Hilbert transform, the Radon transform and its inverse

$$\mathcal{H}\{f\}(x,y) = \mathcal{R}^{-1}\left\{ \begin{bmatrix} \cos\theta \\ \sin\theta \end{bmatrix} \underbrace{(h(t) * f_r(t,\theta))}_{\mathcal{H}\{f_r\}(t;\theta)} \right\}(x,y)$$

with

$$\mathcal{H}\{f_r\}(t;\theta) = -\frac{1}{\pi}\text{P.V.} \int\limits_{\tau\in\mathbb{R}} \frac{f_r(\tau - t, \theta)}{\tau} d\tau$$

as the classical 1D Hilbert transform in Radon space. In other words, the Hilbert transform applies a one-dimensional Hilbert transform to the Radon space representation $f_r(t;\theta)$ of the original signal along the parameter $t \in \mathbb{R}$ for each orientation angle $\theta \in [0,\pi)$ separately.
In the following it will be shown that the first order Hilbert transform can be written in terms of the Radon transform $\mathcal{R}\{\cdot\}$, its inverse $\mathcal{R}^{-1}\{\cdot\}$ and the 1D Hilbert transform.
The proof will be shown in Fourier domain by means of the Fourier slice theorem (FST). The 1D Hilbert transform can be written in Fourier space as

$$H(u) := \mathcal{F}_1\{h\}(u) = \mathbf{i}\,\text{sign}(u),\ u \in \mathbb{R}$$

with

$$\text{sign}(u) := \begin{cases} 1, & u > 0 \\ -1, & u < 0 \\ 0, & u = 0 \end{cases}$$

which can be also written in terms of $\frac{u}{\|u\|} = \text{sign}(u)$ for $u \in \mathbb{R} \setminus \{0\}$ and $\mathbf{i}$ as the imaginary unit of the complex numbers $\mathbb{C}$. The 2D Hilbert transform kernel can be represented in Fourier space by

$$H^{(1)}(u) := \mathcal{F}_2\left\{h^{(1)}\right\}(u) = \mathbf{i}\frac{u}{\|u\|},\ u \in \mathbb{R}^2 \setminus \{(0,0)\}$$

and is written as components in x and y direction

$$H_x(u\, n_\theta) := \mathcal{F}_2\{h_x\}(u\, n_\theta) = \mathbf{i}\frac{u\cos\theta}{\|u\|},\ u \in \mathbb{R} \setminus \{0\}$$

and

$$H_y(u\,n_\theta) := \mathcal{F}_2\left\{h_y\right\}(u\,n_\theta) = \mathbf{i}\frac{u\sin\theta}{\|u\|},\ u \in \mathbb{R}\setminus\{0\}\ .$$

By means of the Fourier slice theorem

$$\mathcal{F}_1\left\{\mathcal{R}\left\{\cdot\right\}\right\}(u,\theta) = \mathcal{F}_2\left\{\cdot\right\}(u\,n_\theta),\ u \in \mathbb{R}$$

with $\mathcal{F}_1\left\{\cdot\right\}(u,\theta) \in \mathbb{C}$ as the 1D partial Fourier transform of a 2D signal in direction of $\theta \in [0, 2\pi)$ and $n_\theta := [\cos\theta, \sin\theta]^T$, it will be shown that the Hilbert transform can be written in terms of the Radon transform as

$$\begin{aligned}
& \mathcal{F}_1\left\{\mathcal{R}\left\{\mathcal{H}\left\{f\right\}\right\}\right\}(u,\theta) \\
= & \begin{bmatrix} \mathcal{F}_1\left\{\mathcal{R}\left\{\mathcal{H}_x\left\{f\right\}\right\}\right\}(u,\theta) \\ \mathcal{F}_1\left\{\mathcal{R}\left\{\mathcal{H}_y\left\{f\right\}\right\}\right\}(u,\theta) \end{bmatrix} \\
= & \begin{bmatrix} \mathcal{F}_2\left\{\mathcal{H}_x\left\{f\right\}\right\}(u\,n_\theta) \\ \mathcal{F}_2\left\{\mathcal{H}_y\left\{f\right\}\right\}(u\,n_\theta) \end{bmatrix} \\
= & \mathcal{F}_2\left\{f\right\}(u\,n_\theta)\begin{bmatrix} H_x(u\,n_\theta) \\ H_y(u\,n_\theta) \end{bmatrix} \\
= & \mathcal{F}_2\left\{f\right\}(u\,n_\theta)\begin{bmatrix} \mathbf{i}\frac{u\cos\theta}{\|u\|} \\ \mathbf{i}\frac{u\sin\theta}{\|u\|} \end{bmatrix} \\
= & \mathbf{i}\ \mathrm{sign}(u)\mathcal{F}_2\left\{f\right\}(u\,n_\theta)\begin{bmatrix} \cos\theta \\ \sin\theta \end{bmatrix} \\
= & \mathcal{F}_1\left\{h\right\}(u)\mathcal{F}_2\left\{f\right\}(u\,n_\theta)\begin{bmatrix} \cos\theta \\ \sin\theta \end{bmatrix} \\
= & \mathcal{F}_1\left\{h\right\}(u)\mathcal{F}_1\left\{\mathcal{R}\left\{f\right\}\right\}(u,\theta)\begin{bmatrix} \cos\theta \\ \sin\theta \end{bmatrix} \\
= & \mathcal{F}_1\left\{h\right\}(u)\mathcal{F}_1\left\{\mathcal{R}\left\{f\right\}\right\}(u,\theta)\begin{bmatrix} \cos\theta \\ \sin\theta \end{bmatrix}
\end{aligned}$$

Because of the existence of the inverse Radon transform $\mathcal{R}^{-1}\left\{\cdot\right\}$, now the relation of the Radon transform and the Hilbert transform follows

$$\mathcal{F}_1\left\{\mathcal{R}\left\{\mathcal{H}\left\{f\right\}\right\}\right\}(u,\theta) = \mathcal{F}_1\left\{h\right\}(u)\mathcal{F}_1\left\{\mathcal{R}\left\{f\right\}\right\}(u,\theta)\begin{bmatrix} \cos\theta \\ \sin\theta \end{bmatrix}$$

$$\begin{aligned}
\Rightarrow\ & \mathcal{R}\left\{\mathcal{H}\left\{f\right\}\right\}(t,\theta) = h(t) * \mathcal{R}\left\{f\right\}(t,\theta)\begin{bmatrix} \cos\theta \\ \sin\theta \end{bmatrix} \\
\Rightarrow\ & \mathcal{H}\left\{f\right\}(x,y) = \mathcal{R}^{-1}\left\{h(t) * \mathcal{R}\left\{f\right\}(t,\theta)\begin{bmatrix} \cos\theta \\ \sin\theta \end{bmatrix}\right\}(x,y)
\end{aligned}$$

which proves the proposition.
Please note that because of the important property $\mathcal{R}\{\mathcal{R}^{-1}\{f\}\} = f$, the n-th order Hilbert transform $\mathcal{H}^{(n)}\{f\}$ of a signal can be easily written as the concatenation of n first order Hilbert transforms expressed in Radon space. This fact is very important for the higher order Hilbert transforms such as the second order Hilbert transform

$$\mathcal{H}^{(2)}\{f\}(x,y) = \mathcal{H}\{\mathcal{H}\{f\}\}(x,y)$$

and the third order Hilbert transform

$$\mathcal{H}^{(3)}\{f\}(x,y) = \mathcal{H}\{\mathcal{H}\{\mathcal{H}\{f\}\}\}(x,y)$$

which will be intensively used in this work.
In case of the second order Hilbert transform the concatenation of the two first order Hilbert transforms can be done componentwise. This will be now demonstrated exemplarily with the $\mathcal{H}^{(2)}_{xx}(x,y)$ component of the second order Hilbert transform. By definition

$$\mathcal{H}_x\{\cdot\}(x,y) = \mathcal{R}^{-1}\left\{\cos\theta(h(t) * \mathcal{R}\{\cdot\})(t;\theta)\right\}(x,y)$$

the second order Hilbert transform can be expressed as a concatenation

$$\begin{aligned}
& \mathcal{H}^{(2)}_{xx}\{f\}(x,y) := \mathcal{H}_x\{\mathcal{H}_x\{f\}\}(x,y) \\
= \; & \mathcal{R}^{-1}\left\{\cos\theta(h(t) * \mathcal{R}\{\mathcal{R}^{-1}\left\{\cos\theta(h(t) * \mathcal{R}\{f\})(t;\theta)\right\}\})(t;\theta)\right\}(x,y) \\
= \; & \mathcal{R}^{-1}\left\{\cos\theta\left(h(t) * \left[\cos\theta\left(h(t) * \mathcal{R}\{f\}\right)(t;\theta)\right]\right)(t;\theta)\right\}(x,y) \\
= \; & \mathcal{R}^{-1}\left\{\cos^2\theta\,\underbrace{(h(t) * h(t))}_{-1} * \mathcal{R}\{f\}(t;\theta)\right\}(x,y) \\
= \; & -\mathcal{R}^{-1}\left\{\cos^2\theta\;\mathcal{R}\{f\}(t;\theta)\right\}(x,y)
\end{aligned}$$

This can be done analogously for all other components of the second order Hilbert transform

$$\begin{aligned}
\mathcal{H}^{(2)}_{xx}\{f\}(x,y) &= -\mathcal{R}^{-1}\left\{\cos^2\theta\; f_r(t;\theta)\right\}(x,y) \\
\mathcal{H}^{(2)}_{xy}\{f\}(x,y) &= -\mathcal{R}^{-1}\left\{\cos\theta\sin\theta\; f_r(t;\theta)\right\}(x,y) \\
\mathcal{H}^{(2)}_{yy}\{f\}(x,y) &= -\mathcal{R}^{-1}\left\{\sin^2\theta\; f_r(t;\theta)\right\}(x,y)
\end{aligned}$$

with $f_r(t;\theta) := \mathcal{R}\{f\}(t;\theta)$.
The third order Hilbert transform can be expressed as a concatenation of

three first order Hilbert transforms

$$\begin{aligned}
\mathcal{H}^{(3)}_{xxx}\{f\}(x,y) &= -\mathcal{R}^{-1}\left\{\cos^3\theta\ (h(t)*f_r(t;\theta))\right\}(x,y) \\
\mathcal{H}^{(3)}_{xxy}\{f\}(x,y) &= -\mathcal{R}^{-1}\left\{\cos^2\theta\sin\theta\ (h(t)*f_r(t;\theta))\right\}(x,y) \\
\mathcal{H}^{(3)}_{xyy}\{f\}(x,y) &= -\mathcal{R}^{-1}\left\{\cos\theta\sin^2\theta\ (h(t)*f_r(t;\theta))\right\}(x,y) \\
\mathcal{H}^{(3)}_{yyy}\{f\}(x,y) &= -\mathcal{R}^{-1}\left\{\sin^3\theta\ (h(t)*f_r(t;\theta))\right\}(x,y)
\end{aligned}$$

since $h(t)*h(t)*h(t) = -h(t)$.

Chapter 5

Poisson Scale Space

Since all signals $f \in L_2(\Omega, \mathbb{R})$ with $\Omega \subseteq \mathbb{R}^2$ can be decomposed into their corresponding Fourier series [3], for each frequency a certain amplitude and phase can be obtained. Therefore the local frequency of interest must be filtered out locally of the original signal. The frequency corresponds to the so called scale space parameter $s > 0$. The representation of a signal f in monogenic scale space [12] can be computed by 2D convolution $*$ with the 2D Poisson filter kernel $p(x, y; s)$ in spatial domain. The kernel of the Poisson operator $\mathcal{P}\{\cdot\}(x, y; s)$,

$$p(x, y; s) := \frac{s}{2\pi \left(s^2 + x^2 + y^2\right)^{\frac{3}{2}}} ,$$

is a low pass filter which maps the original signal to the Poisson scale space f_p,

$$f_p := \mathcal{P}\{f\}(x, y; s) := (p * f)(x, y; s) .$$

Besides, there are two conjugate Poisson kernels as the scale space representation of the Hilbert transform.

$$\begin{aligned} f_x &:= \mathcal{Q}_x\{f\}(x, y; s) := (q_x * f)(x, y; s) := (h_x * p * f)(x, y; s) \\ f_y &:= \mathcal{Q}_y\{f\}(x, y; s) := (q_y * f)(x, y; s) := (h_y * p * f)(x, y; s) \end{aligned}$$

with the convolution kernels in spatial domain

$$\begin{aligned} q_x(x, y; s) &= \frac{x}{2\pi \left(s^2 + x^2 + y^2\right)^{\frac{3}{2}}} \\ q_y(x, y; s) &= \frac{y}{2\pi \left(s^2 + x^2 + y^2\right)^{\frac{3}{2}}} . \end{aligned}$$

(see figure 5.1). The vector $[f_p, f_x, f_y]^T$ constitutes the monogenic scale space of the original signal f. For signal analysis a small passband of the original signal spectrum must be created. This can be done by the difference of Poisson (DoP) operator kernel

$$p(x, y; s_c, s_f) := p(x, y; s_f) - p(x, y; s_c) ,$$

which is defined by the coarse scale space parameter s_c and the fine scale space parameter s_f with $s_c > s_f > 0$.

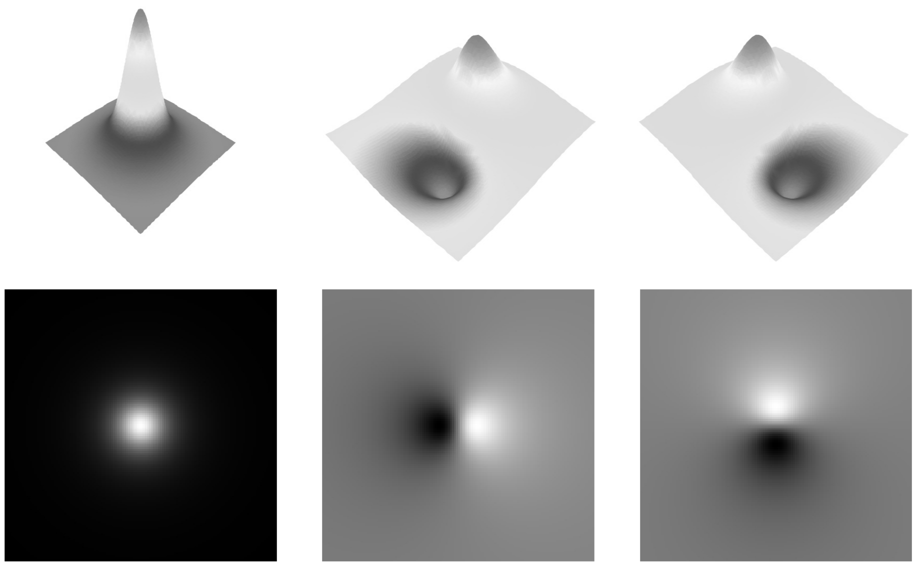

Figure 5.1: From left to right: Poisson convolution kernel $p(x, y; s)$ and conjugate Poisson convolution kernels $q_x(x, y; s)$ and $q_y(x, y; s)$ in spatial domain for a certain scale space parameter $s > 0$.

5.1 Second Order Hilbert Transform

In order to use the higher order Hilbert kernels in the monogenic scale space concept their Poisson transforms in spatial domain are needed. They can be obtained by convolution of the kernels with the Poisson kernel in $\mathbb{R}^2$. We will demonstrate that in this section for the second order Hilbert transform [15] and in the next section for the third order Hilbert transform.
To calculate the convolution in frequency space, the Fourier transforms $\mathcal{F}\{\cdot\}(u)$ of the convolution kernels $h^{(2)}(x, y)$ and $p(x, y; s)$ are considered. According to the convolution theorem, the convolution in spatial domain corresponds to a multiplication in Fourier space. The Fourier transform of $h^{(2)}(x, y)$ results

in the multiplier

$$\mathcal{F}\{h^{(2)}\}(u) = -\frac{\overline{u}}{u}$$

with $u := u_1 + \mathbf{i}u_2 \in \mathbb{C}$ and the conjugate $\overline{u} := u_1 - \mathbf{i}u_2$. The Fourier transform of the Poisson convolution kernel $p(x, y, ; s)$ is obtained as

$$\mathcal{F}\{p\}(u; s) = e^{-2\pi\|u\|s}$$

By representing the frequency domain in polar coordinates, with $u = r[\cos\theta + \mathbf{i}\sin\theta]$ and $z := x + \mathbf{i}y := k[\cos\varphi + \mathbf{i}\sin\varphi]$, the frequency transfer functions of these kernels read

$$\mathcal{F}\{h^{(2)}\}(u) = -\frac{e^{-\mathbf{i}\theta}}{e^{\mathbf{i}\theta}} = -e^{-\mathbf{i}2\theta}$$

and

$$\mathcal{F}\{p\}(u; s) = e^{-2\pi\, rs}\ .$$

Using the polar coordinate representation of the inverse two-dimensional Fourier transform to obtain the spatial domain representation of the kernels yields

$$\begin{aligned}
(p * h^{(2)})(z; s) &= \mathcal{F}^{-1}\{-e^{-2\pi rs}e^{-\mathbf{i}2\theta}\}(z; s) \\
&= 2\pi \int_{r=0}^{\infty}\int_{\theta=0}^{2\pi} -e^{-2\pi rs}e^{-\mathbf{i}2\theta}e^{\mathbf{i}2\pi kr\cos(\theta-\varphi)} r\ d\theta\ dr \\
&= 2\pi \int_{r=0}^{\infty}\int_{\theta=0}^{2\pi} -e^{-2\pi rs}e^{-\mathbf{i}2(\theta+\varphi)}e^{\mathbf{i}2\pi kr\cos(\theta-\varphi+\varphi)} r\ d\theta\ dr \\
&= -2\pi e^{-\mathbf{i}2\varphi}\int_{r=0}^{\infty} e^{-2\pi rs}\underbrace{\left[\int_{\theta=0}^{2\pi} e^{-\mathbf{i}2\theta}e^{-\mathbf{i}2\pi kr\cos\theta}\ d\theta\right]}_{=J_2(2\pi kr)} r\ dr \\
&= -2\pi e^{-\mathbf{i}2\varphi}\int_{r=0}^{\infty} e^{-2\pi rs}J_2(2\pi kr) r\ dr
\end{aligned}$$

where J_2 is a Bessel function of the first kind and second order. In the following the abbreviations $\alpha := 2\pi s$ and $\beta := 2\pi k$ will be used. J_2 can be written according to the recurrence relation for Bessel functions as

$$J_2(2\pi kr) = J_2(\beta r) = \frac{2}{\beta r}J_1(\beta r) - J_0(\beta r)$$

since the recurrence relation reads

$$J_\nu(x) = \frac{2(\nu-1)}{x} J_{\nu-1}(x) - J_{\nu-2}(x) \ .$$

These results lead to

$$(h^{(2)} * p)(z;s) = -2\pi e^{-\mathbf{i}2\varphi} \int\limits_{r=0}^{\infty} e^{-\alpha r} J_2(2\pi k r) r \ dr$$

$$\begin{aligned}
= & \ -2\pi e^{-\mathbf{i}2\varphi} \int\limits_{r=0}^{\infty} e^{-\alpha r} \frac{2}{\beta r} J_1(\beta r) r \ dr \\
+ & \ 2\pi e^{-\mathbf{i}2\varphi} \int\limits_{r=0}^{\infty} e^{-\alpha r} J_0(\beta r) r \ dr \\
= & \ -2\pi e^{-\mathbf{i}2\varphi} \left[\frac{2}{\beta} \int\limits_{r=0}^{\infty} e^{-\alpha r} J_1(\beta r) dr - \int\limits_{r=0}^{\infty} e^{-\alpha r} J_0(\beta r) r \ dr \right] \ .
\end{aligned}$$

According to common integral tables [17] one obtains the evaluation of the two Bessel integrals as

$$\frac{2}{\beta} \int\limits_{r=0}^{\infty} e^{-\alpha r} J_1(\beta r) \ dr = \frac{2\left[\sqrt{\alpha^2+\beta^2} - \alpha\right]}{\beta^2 \sqrt{\alpha^2+\beta^2}}$$

since

$$\int\limits_{r=0}^{\infty} e^{-\alpha r} J_\nu(\beta r) \ dr = \frac{\left[\sqrt{\alpha^2+\beta^2} - \alpha\right]^\nu}{\beta^\nu \sqrt{\alpha^2+\beta^2}}$$

(see [17], page 694 for $\nu = 1$) and

$$\int\limits_{r=0}^{\infty} e^{-\alpha r} J_0(\beta r) r \ dr = \frac{2\alpha \Gamma\left(\frac{3}{2}\right)}{\sqrt{\pi}(\alpha^2+\beta^2)^{\frac{3}{2}}} = \frac{\alpha}{(\alpha^2+\beta^2)^{\frac{3}{2}}}$$

since $\Gamma\left(\frac{3}{2}\right) = \frac{\sqrt{\pi}}{2}$ and

$$\int\limits_{r=0}^{\infty} e^{-\alpha r} J_\nu(\beta r) r^{\nu+1} \ dr = \frac{2\alpha(2\beta)^\nu \Gamma\left(\nu+\frac{3}{2}\right)}{\sqrt{\pi}(\alpha^2+\beta^2)^{\nu+\frac{3}{2}}}$$

(see [17], page 702 for $\nu = 0$). Plugging these results in the equations above results in

$$(h^{(2)} * p)(z;s) = -2\pi e^{-\mathbf{i}2\varphi} \int\limits_{r=0}^{\infty} e^{-\alpha r} J_2(2\pi k r) r \, dr$$

$$= \frac{s(2s^2 + 3\|z\|^2) - 2(s^2 + \|z\|^2)^{\frac{3}{2}}}{2\pi \|z\|^4 (s^2 + \|z\|^2)^{\frac{3}{2}}} (x^2 - 2\mathbf{i}xy - y^2)$$

with

$$e^{-\mathbf{i}2\varphi} = \left[e^{-\mathbf{i}\varphi}\right]^2 = \left[\frac{\overline{z}}{\|z\|}\right]^2 = \frac{(x - \mathbf{i}y)^2}{\|z\|^2} = (x^2 - 2\mathbf{i}xy - y^2)\frac{1}{\|z\|^2} \; .$$

These results lead to the three different 2D convolution kernels in spatial domain of the second order Hilbert transform in monogenic scale space

$$\begin{bmatrix} q_{xx} \\ q_{xy} \\ q_{yy} \end{bmatrix} (x, y; s) := \begin{bmatrix} h_{xx} * p \\ h_{xy} * p \\ h_{yy} * p \end{bmatrix} (x, y; s) =$$
$$\frac{s(2s^2 + 3(x^2 + y^2)) - 2(s^2 + x^2 + y^2)^{\frac{3}{2}}}{2\pi (x^2 + y^2)^2 (s^2 + x^2 + y^2)^{\frac{3}{2}}} \begin{bmatrix} x^2 \\ xy \\ y^2 \end{bmatrix}$$

(see figure 5.2).

5.2 Third Order Hilbert Transform

The Fourier transform of the convolution kernel $h^{(3)}(x, y)$ results in the multiplier

$$\mathcal{F}\{h^{(3)}\}(u) = -e^{-\mathbf{i}3\theta} \; .$$

In the same way as for the second order Hilbert transform we now compute the representation of the third order Hilbert transform in monogenic scale

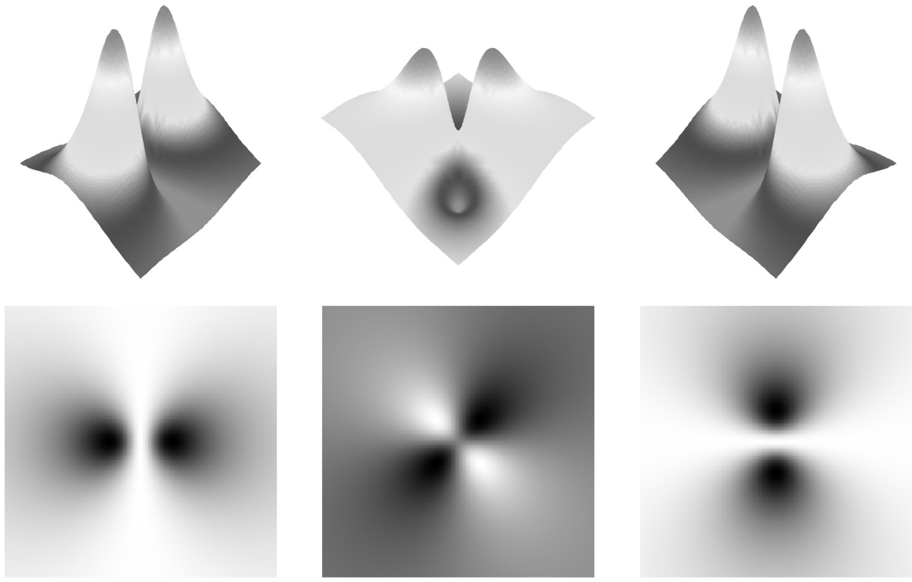

Figure 5.2: From left to right: Second order Hilbert transform convolution kernels in spatial domain $q_{xx}(x, y; s)$, $q_{xy}(x, y; s)$ and $q_{yy}(x, y; s)$ for a certain scale space parameter $s > 0$.

space.

$$\begin{aligned}
(h^{(3)} * p)(z; s) &= \mathcal{F}^{-1}\{-e^{-2\pi rs}e^{-\mathbf{i}3\theta}\}(z; s) \\
&= 2\pi \int\limits_{r=0}^{\infty}\int\limits_{\theta=0}^{2\pi} -e^{-2\pi rs}e^{-\mathbf{i}3\theta}e^{\mathbf{i}2\pi kr\cos(\theta-\varphi)}r\ d\theta\ dr \\
&= 2\pi \int\limits_{r=0}^{\infty}\int\limits_{\theta=0}^{2\pi} -e^{-2\pi rs}e^{-\mathbf{i}3(\theta+\varphi)}e^{\mathbf{i}2\pi kr\cos(\theta-\varphi+\varphi)}r\ d\theta\ dr \\
&= -2\pi e^{-\mathbf{i}3\varphi}\int\limits_{r=0}^{\infty} e^{-2\pi rs}\underbrace{\left[\int\limits_{\theta=0}^{2\pi} e^{-\mathbf{i}3\theta}e^{-\mathbf{i}2\pi kr\cos\theta}\ d\theta\right]}_{=J_3(2\pi kr)} r\ dr \\
&= -2\pi e^{-\mathbf{i}3\varphi}\int\limits_{r=0}^{\infty} e^{-2\pi rs}J_3(2\pi kr)r\ dr
\end{aligned}$$

with

$$J_3(2\pi kr) = J_3(\beta r) = \frac{4}{\beta r}J_2(\beta r) - J_1(\beta r)$$

and with

$$\int_{r=0}^{\infty} e^{-\alpha r} J_\nu(\beta r) r^\nu \, dr = \frac{(2\beta)^\nu \Gamma\left(\nu + \frac{1}{2}\right)}{\sqrt{\pi}(\alpha^2 + \beta^2)^{\nu + \frac{1}{2}}}$$

The 2D convolution kernels in spatial domain of the third order Hilbert transform in monogenic scale space read (see figure 5.3)

$$\begin{bmatrix} q_{xxx} \\ q_{xxy} \\ q_{xyy} \\ q_{yyy} \end{bmatrix} (x, y; s) := \begin{bmatrix} h_{xxx} * p \\ h_{xxy} * p \\ h_{xyy} * p \\ h_{yyy} * p \end{bmatrix} (x, y; s) =$$

$$\frac{4s^2(2s^2 + 3(x^2 + y^2)) + 3(x^2 + y^2)^2 - 8s(s^2 + x^2 + y^2)^{\frac{3}{2}}}{(x^2 + y^2)^3 (s^2 + x^2 + y^2)^{\frac{3}{2}}} \begin{bmatrix} x^3 \\ x^2 y \\ x y^2 \\ y^3 \end{bmatrix} .$$

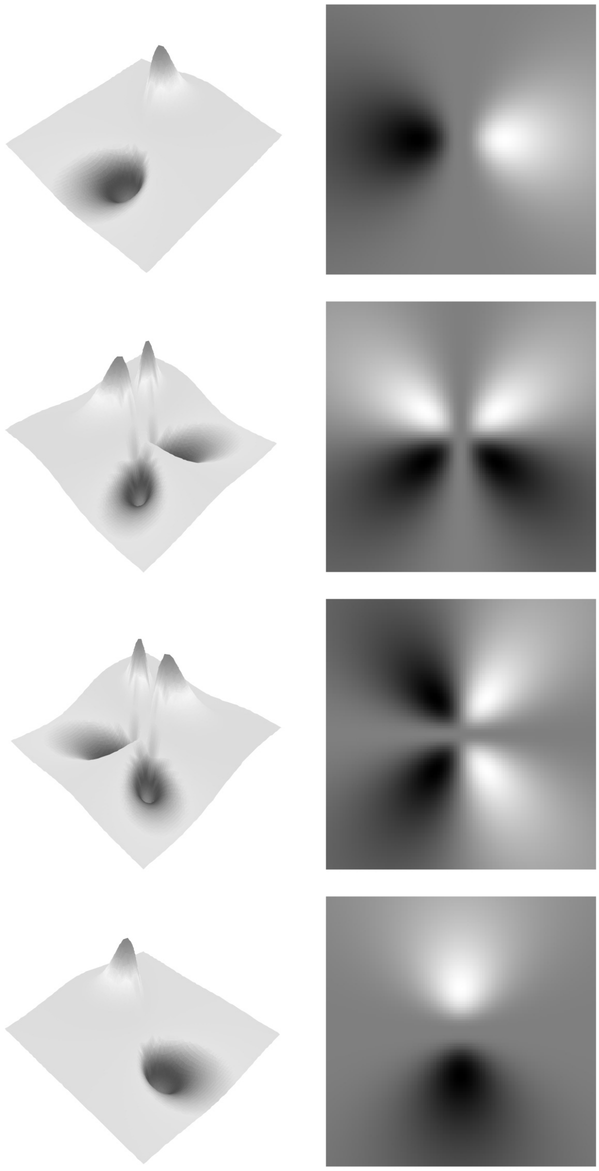

Figure 5.3: From top to bottom: Third order Hilbert transform convolution kernels in spatial domain $q_{xxx}(x, y; s)$, $q_{xxy}(x, y; s)$, $q_{xyy}(x, y; s)$ and $q_{yyy}(x, y; s)$ for a certain scale space parameter $s > 0$.

Chapter 6

i1D Signal Analysis

The i1D signal model (which is an arbitrary orientated 1D signal in 2D domain) in Poisson scale space for each scale parameter $s > 0$ reads

$$\mathcal{P}\{f\}(x, y; s) = a_s \cos(x \cos\theta_s + y \sin\theta_s + \phi_s) \ .$$

We will use the abbreviations $a := a_s$, $\theta := \theta_s$ and $\phi := \phi_s$ in the following. The resulting local signal model at the origin $(0, 0) \in \mathbb{R}^2$ of the local coordinate system reads

$$f_p = \mathcal{P}\{f\}(0, 0; s) = a \cos\phi \ .$$

For a real 2D signal $f \in L_2(\Omega, \mathbb{R})$ with $\Omega \subseteq \mathbb{R}^2$ the 2D monogenic signal [11] can be defined in vector notation

$$\begin{bmatrix} f_p \\ f_x \\ f_y \end{bmatrix} = \frac{1}{2\pi} \int\limits_{(\mu,\nu)\in\mathbb{R}^2} \frac{f(\mu, \nu)}{(s^2 + (x-\mu)^2 + (y-\nu)^2)^{\frac{3}{2}}} \begin{bmatrix} s \\ x-\mu \\ y-\nu \end{bmatrix} d(\mu, \nu)$$

in monogenic scale space for each scale parameter $s > 0$. The monogenic signal can only be interpreted for i1D signals.

6.1 First Order Hilbert Transform in Radon Space

By the relation of the 2D Radon transform $f_r(t, \theta) := \mathcal{R}\{\mathcal{P}\{f\}\}(t, \theta)$ [23] of the original signal f (see figure 6.1), the inverse 2D Radon transform $\mathcal{R}^{-1}\{\cdot\}(x, y)$ and the first order Hilbert transform (generalized Hilbert transform)

$$\begin{bmatrix} f_x \\ f_y \end{bmatrix} = \mathcal{R}^{-1}\left\{ \begin{bmatrix} \cos\theta \\ \sin\theta \end{bmatrix} (h(t) * f_r(t; \theta)) \right\}(x, y; s)$$

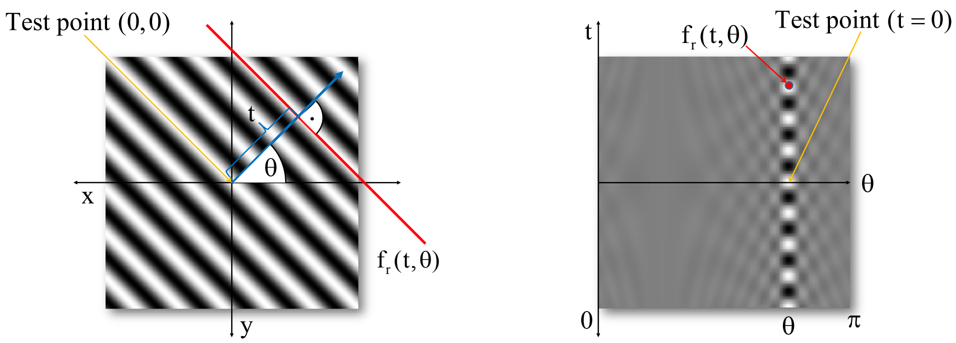

Figure 6.1: Left figure: i1D signal f_p in spatial domain with orientation θ_m and local phase $\phi = 0$ at the origin $(0,0) \in \mathbb{R}^2$ of the applied local coordinate system. Right figure: i1D signal f_p in Radon space. Each point in Radon space represents the integral in spatial domain on a line which is uniquely defined by the minimal distance $t \in \mathbb{R}$ to the origin and the orientation $\theta \in [0, \pi)$. The Radon transform of the Poisson filtered signal will be abbreviated by $f_r(t, \theta) := \mathcal{R}\{\mathcal{P}\{f\}\}(t, \theta)$.

and by the one-dimensional Hilbert transform

$$(h(t) * g(t; s))\,(0; s) = a \sin \phi$$

with the partial 1D function in direction θ

$$g(t; s) := \mathcal{P}\{f\}(t \cos \theta, t \sin \theta; s)$$

and the one-dimensional Hilbert transform kernel $h(t) = \frac{1}{\pi t}$ it can be shown that the conjugate part of the monogenic signal results in

$$\begin{aligned} f_x = \mathcal{Q}_x\{f\}(0, 0; s) &= a \cos \theta \sin \phi \\ f_y = \mathcal{Q}_y\{f\}(0, 0; s) &= a \sin \theta \sin \phi \,. \end{aligned}$$

for all i1D signals.

6.2 Interpretation

Now the monogenic signal vector $[f_p, f_x, f_y]^T \in \mathbb{R}^3$ 6.2 can be used to solve for the unknown local amplitude $a \in \mathbb{R}_+$, the local orientation $\theta \in [0, \pi)$ and the local phase $\phi \in [0, \pi)$

$$\begin{aligned}
\theta &= \arctan \frac{f_y}{f_x} \\
\phi &= \operatorname{atan2}\left(\sqrt{f_x^2 + f_y^2}, f_p\right) \\
a &= \sqrt{f_p^2 + f_x^2 + f_y^2} \ .
\end{aligned}$$

The proof becomes easy with the previous results of the 2D Radon space expression

$$\begin{aligned}
f_p &= a \cos \phi \\
f_x &= a \cos \theta \sin \phi \\
f_y &= a \sin \theta \sin \phi \ .
\end{aligned}$$

At phase positions $\phi = k\pi$ for all $k \in \mathbb{Z}$ the orientation can not be evaluated. Note that the local features must be evaluated for each scale space parameter $s > 0$ since in general the signal consists locally of different frequency components. Now the problem of i1D signal analysis is totally solved. The next step will be the modeling of i1D and i2D signals and the exact solution for their parameters. Abstractly spoken, local signal analysis is the solution of its corresponding *inverse problem* [1].

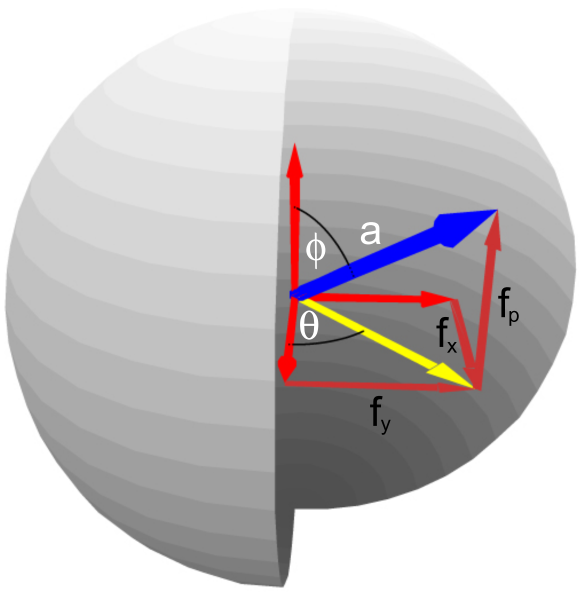

Figure 6.2: Geometric illustration and interpretation of the 2D monogenic signal vector $[f_p, f_x, f_y]^T$ in 3D Euclidean space.

Chapter 7

i1D and i2D Signal Analysis

The monogenic signal can be used to analyze i1D signals such as lines and edges. Unfortunately the monogenic signal can not distinguish between i1D and i2D signals. The most interesting class of signals is the set of i2D signals. In general i2D signals can only be described by an infinity number of superimposed i1D signals. Therefore, a signal model must be defined which subsumes all i1D signals and also the most interesting i2D signal structures (such as corners and junctions in the case of image signals). In the case of two superimposed i1D signals this signal model reads

$$\mathcal{P}\{f\}(x, y; s) = \sum_{i=1}^{2} a_s \cos(x \cos\theta_{i,s} + y \sin\theta_{i,s} + \phi_s)$$

with the abbreviations $a := a_s$, $\theta_i := \theta_{i,s}$ and $\phi := \phi_s$. The resulting local signal model at the origin $(x, y) := (0, 0)$ of the test point is given by

$$f_p := 2a \cos\phi := 2a_s \cos\phi_s = \mathcal{P}\{f\}(0, 0; s) \ .$$

Note that equal amplitudes and phases are assumed for both i1D signals. In case of $\theta_1 \mod \pi = \theta_2 \mod \pi$ this is the ordinary i1D signal model. The i1D signal model has three unknown structure features (phase, amplitude and orientation) and the monogenic signal vector consists of three signal components $[f_p, f_x, f_y]^T \in \mathbb{R}^3$ to solve the system of equations. Since the i2D signal model consists of four unknowns, more signal components are required. Therefore, the next step will be the exploitation of the components of the second order Hilbert transform $[\mathcal{Q}_{xx}, \mathcal{Q}_{xy}, \mathcal{Q}_{yy}]^T$ which are related to the entries of the Hessian matrix. Motivated by the first and second order derivatives of the Weingarten map $\left[\frac{\partial}{\partial x}, \frac{\partial}{\partial y}, \frac{\partial^2}{\partial x^2}, \frac{\partial^2}{\partial xy}, \frac{\partial^2}{\partial y^2}\right]^T$ known from differential geometry [9], here the first and second order Hilbert transform operators will be used for signal analysis $[\mathcal{Q}_x, \mathcal{Q}_y, \mathcal{Q}_{xx}, \mathcal{Q}_{xy}, \mathcal{Q}_{yy}]^T$. Analogously to the pure i1D signal model, the first order Hilbert transform of the i1D/i2D signal model reads

$$\begin{bmatrix} f_x \\ f_y \end{bmatrix} = \sum_{i=1}^{2} a \sin\phi \begin{bmatrix} \cos\theta_i \\ \sin\theta_i \end{bmatrix}$$

at the origin $(0,0) \in \mathbb{R}^2$ of the local coordinate system.

7.1 Second Order Hilbert Transform in Radon Space

Same as with the first order Hilbert transform the second order Hilbert transform of the i1D / i2D signal can be also evaluated by the relation of the Radon transform (see figure 7.1) and the Hilbert transform by concatenation of two first order Hilbert transforms

$$\begin{bmatrix} f_{xx} \\ f_{xy} \\ f_{yy} \end{bmatrix} = -\mathcal{R}^{-1} \left\{ \begin{bmatrix} \cos^2\theta \\ \sin\theta\cos\theta \\ \sin^2\theta \end{bmatrix} f_r(t,\theta) \right\} (x, y; s)$$

since $(h * h)(t) = -1$. The second order Hilbert transform of the assumed signal model results in

$$\begin{bmatrix} f_{xx} \\ f_{xy} \\ f_{yy} \end{bmatrix} = \sum_{i=1}^{2} a \cos\phi \begin{bmatrix} \cos^2\theta_i \\ \frac{1}{2}\sin(2\theta_i) \\ \sin^2\theta_i \end{bmatrix}$$

The first conclusion is the reconstruction of the Poisson filtered original signal

$$f_{xx} + f_{yy} = 2a\cos\phi = f_p \; .$$

With these results the system of equations has to be solved and the four unknown local features such as amplitude, orientation, phase and apex angle have to be derived.

7.2 Third Order Hilbert Transform in Radon Space

Analogously to the second order Hilbert transform of the signal f the third order Hilbert transform expressed in Radon space reads

$$\begin{bmatrix} f_{xxx} \\ f_{xxy} \\ f_{xyy} \\ f_{yyy} \end{bmatrix} = -\mathcal{R}^{-1}\left\{\begin{bmatrix} \cos^3\theta \\ \cos^2\theta\sin\theta \\ \cos\theta\sin^2\theta \\ \sin^3\theta \end{bmatrix}(h(t) * f_r(t;\theta))\right\}(x, y; s)$$

since $(h*h*h)(t) = -h(t)$ and with the abbreviation $f_r(t,\theta) := \mathcal{R}\{\mathcal{P}\{f\}\}(t,\theta)$. For the given signal model the third order Hilbert transform results in the following system of equations

$$\begin{bmatrix} f_{xxx} \\ f_{xxy} \\ f_{xyy} \\ f_{yyy} \end{bmatrix} = \sum_{i=1}^{2} a\sin\phi \begin{bmatrix} \cos^3\theta_i \\ \cos^2\theta_i\sin\theta_i \\ \cos\theta_i\sin^2\theta_i \\ \sin^3\theta_i \end{bmatrix}$$

with the first obvious result, namely, that the first order Hilbert transform can be reconstructed

$$\begin{aligned} f_{xxx} + f_{xyy} &= f_x \\ f_{xxy} + f_{yyy} &= f_y \ . \end{aligned}$$

7.3 Hybrid Matrix Geometric Algebra

It has been shown that the monogenic signal can be analyzed as a vector in Euclidean space. Now a generalized concept of the monogenic signal representation will be presented by analyzing not a vector but a so called multivector in conformal space. According to [28] each Clifford number valued matrix $M \in M(2, \mathbb{R}_3)$ with $\mathbb{R}_3 := Cl(\mathbb{R}^3)$ can be mapped to a multivector $m \in \mathbb{R}_{4,1}$ of the Clifford algebra [8] $\mathbb{R}_{4,1} := Cl(\mathbb{R}^{4,1})$ with the set of generating basis vectors

$$B := \{\mathbf{e}_1, \mathbf{e}_2, \mathbf{e}_3, \mathbf{e}_+, \mathbf{e}_-\}$$

which results in the total number of $\left\|2^B\right\| = 32$ basis multivectors with 2^B as the powerset of the set B. The basis vectors have the properties

$$\mathbf{e}_1^2 = \mathbf{e}_2^2 = \mathbf{e}_3^2 = \mathbf{e}_+^2 = 1, \quad \mathbf{e}_-^2 = -1$$

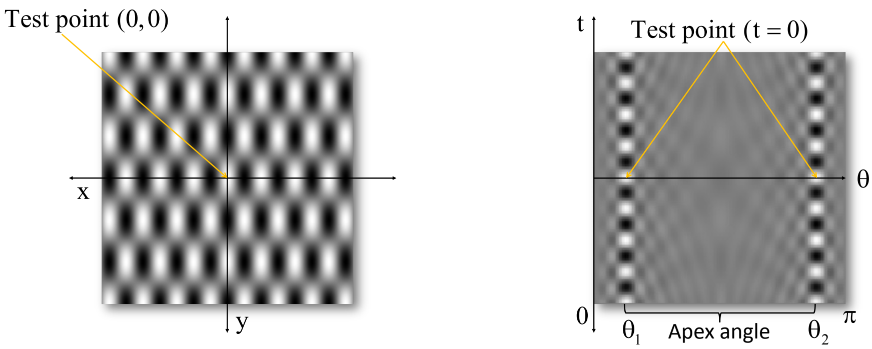

Figure 7.1: Left figure: The i2D checkerboard signal in spatial domain with orientations θ_1, θ_2 and local phase $\phi = 0$ at the test point $(x, y) := (0, 0)$ at the origin of the local coordinate system. Right figure: The i2D signal is separated into two independent i1D signals with different orientations and same phase at $t = 0$ in Radon space.

and

$$\mathbf{e}_i\mathbf{e}_j = -\mathbf{e}_j\mathbf{e}_i, \quad i, j \in \{1, 2, 3, +, -\}, \; i \neq j \; .$$

We will use the abbreviation

$$\mathbf{e}_{ij} := \mathbf{e}_i\mathbf{e}_j \; .$$

Note that the basis vector $\mathbf{e}_+$ extends the three dimensional Euclidean space spanned by $\{\mathbf{e}_1, \mathbf{e}_2, \mathbf{e}_3\}$ to the conformal space and $\mathbf{e}_-$ extends the conformal space to the homogeneous conformal space. In literature the homogenous conformal space will be abbreviated by conformal space. Since we use the Clifford algebra for geometric interpretation, Clifford algebra can be called geometric algebra. As a direct result of [28] each Clifford valued 2×2-matrix of the form

$$M := \begin{bmatrix} M_{11} & M_{12} \\ M_{21} & M_{22} \end{bmatrix} \in M(2, \mathbb{R}_3)$$

can be mapped to its corresponding multivector $m := \varphi(M) \in \mathbb{R}_{4,1}$ in conformal (homogeneous) space [27] by the following isomorphism

$$\varphi(M) := M_{11}u_+ + M_{12}u_+\mathbf{e}_+ + M_{21}^\star u_-\mathbf{e}_+ + M_{22}^\star u_-$$

with

$$M_{ij}^\star := \langle M_{ij}\rangle_0 - \langle M_{ij}\rangle_1 + \langle M_{ij}\rangle_2 - \langle M_{ij}\rangle_3$$

as the *inversion* of the multivector

$$M_{ij} = \sum_{\nu=0}^{3} \langle M_{ij}\rangle_\nu \; \in \mathbb{R}_3$$

for $i, j \in \{1, 2\}$ with the grade n projector $\langle \cdot \rangle_n$ [25] and

$$
\begin{aligned}
u_+ &:= \frac{1}{2} + \frac{1}{2}\mathbf{e}_{+-} \\
u_- &:= \frac{1}{2} - \frac{1}{2}\mathbf{e}_{+-} \\
u_+\mathbf{e}_+ &:= \frac{1}{2}\left[\mathbf{e}_+ - \mathbf{e}_-\right] = -\mathbf{e}_0 \\
u_-\mathbf{e}_+ &:= \frac{1}{2}\left[\mathbf{e}_+ + \mathbf{e}_-\right] = \frac{1}{2}\mathbf{e} \, .
\end{aligned}
$$

This results in the general isomorphism

$$
\begin{aligned}
\varphi(M) &= \frac{1}{2}\left[M_{11} + M_{22}^{\star}\right] \\
&+ \frac{1}{2}\left[M_{21}^{\star} + M_{12}\right]\mathbf{e}_+ \\
&+ \frac{1}{2}\left[M_{21}^{\star} - M_{12}\right]\mathbf{e}_- \\
&+ \frac{1}{2}\left[M_{11} - M_{22}^{\star}\right]\mathbf{e}_{+-}
\end{aligned}
$$

Since the matrix M is isomorphic to the multivector m, the algebra is called a hybrid matrix geometric algebra (HMGA).
Motivated by the Hessian matrix (known from differential geometry) [1]the second order partial derivatives will be substituted by the second order Hilbert transforms in the corresponding directions

$$
M := \begin{bmatrix} f_{xx} & f_{xy} \\ f_{xy} & f_{yy} \end{bmatrix} := \begin{bmatrix} \mathcal{Q}_{xx}\{f\}(0,0;s) & \mathcal{Q}_{xy}\{f\}(0,0;s) \\ \mathcal{Q}_{xy}\{f\}(0,0;s) & \mathcal{Q}_{yy}\{f\}(0,0;s) \end{bmatrix} .
$$

The isomorphic multivector in conformal space reads

$$
m := \varphi(M) = \underbrace{\frac{1}{2}\left[f_{xx} + f_{yy}\right]}_{=:f_s} + \underbrace{f_{xy}}_{=:f_+}\mathbf{e}_+ + \underbrace{\frac{1}{2}\left[f_{xx} - f_{yy}\right]}_{=:f_{+-}}\mathbf{e}_{+-}
$$

with f_s as the scalar part, f_+ as the vector part and f_{+-} as the bivector part. Please note that $f_s \equiv \frac{1}{2} f_p$. This multivector valued signal representation is delivered by a set of three convolution kernels (see figure 7.2).

[1]The Hessian matrix in Gaussian scale space $\mathcal{G}\{\cdot\}(x, y; s)$ reads

$$
M_{\mathrm{Hesse}} := \begin{bmatrix} \frac{\partial^2}{\partial x^2}\mathcal{G}\{f\}(0,0;s) & \frac{\partial^2}{\partial xy}\mathcal{G}\{f\}(0,0;s) \\ \frac{\partial^2}{\partial xy}\mathcal{G}\{f\}(0,0;s) & \frac{\partial^2}{\partial y^2}\mathcal{G}\{f\}(0,0;s) \end{bmatrix}
$$

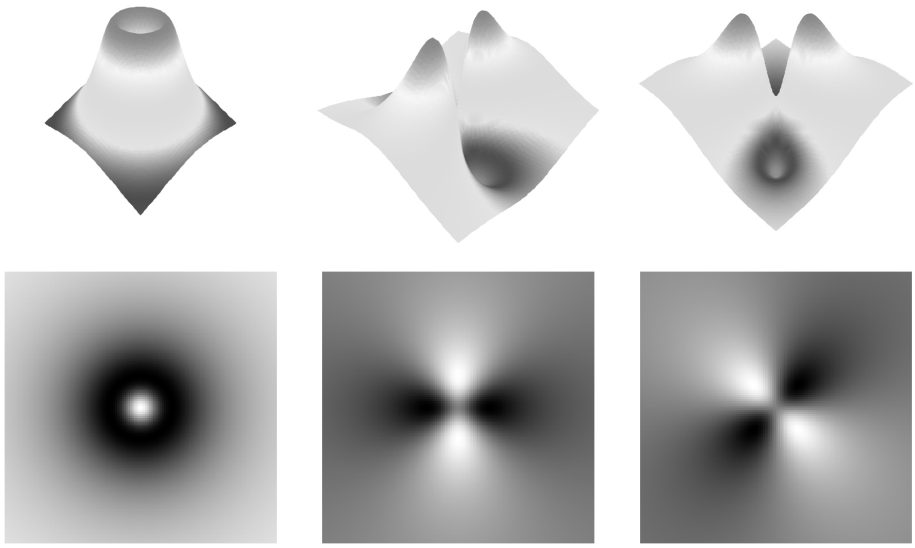

Figure 7.2: From left to right: Convolution kernels which deliver f_s, f_{+-} and f_+ for a certain scale space parameter $s > 0$ in spatial domain.

7.4 Interpretation

The main advantage of the representation in the HMGA is the interpretation of the resulting multivector valued signal m. This new multivector in conformal space is more powerful than the classical vector valued representation in Euclidean space of signals.

7.4.1 Geometrical Signal Features

The local features which determine the signal in scale space will be separated in geometrical features and structural features. The geometrical features are the mean orientation and the rotationally invariant apex angle.

Mean Orientation

The mean orientation [26] reads

$$\theta_m := \frac{\theta_1 + \theta_2}{2} = \frac{1}{2} \arctan \frac{f_+}{f_{+-}} .$$

In contrast to the monogenic signal the mean orientation in conformal space can be evaluated also at phase positions $\phi = k\pi$ for all $k \in \mathbb{Z}$ where the orientation of the monogenic signal $\frac{\theta_1+\theta_2}{2} = \arctan \frac{f_y}{f_x}$ is not defined.

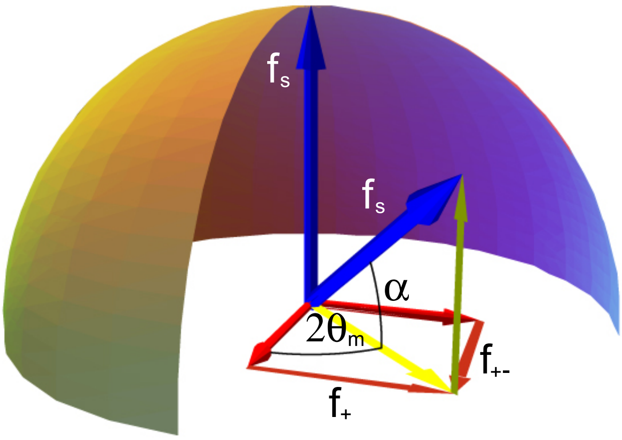

Figure 7.3: Geometric interpretation of the mean orientation θ_m and the apex angle α.

Apex Angle

The apex angle α (also deviation angle, opening angle or intersection angle) reads

$$
\begin{aligned}
\alpha &:= \theta_1 - \theta_2 \\
&= \arccos \frac{\sqrt{f_+^2 + f_{+-}^2}}{\|f_s\|} \\
&= \arctan \frac{\sqrt{f_s^2 - [f_+^2 + f_{+-}^2]}}{\sqrt{f_+^2 + f_{+-}^2}} \\
&= \arctan \frac{\sqrt{\det M}}{\sqrt{f_+^2 + f_{+-}^2}}
\end{aligned}
$$

with the determinant $\det M = f_{xx} f_{yy} - f_{xy}^2$ of the real valued matrix M. The apex angle [2] is a very important rotationally invariant local feature since it is zero iff the underlying structure is of intrinsic dimension one.

[2]Note that the apex angle of phase based image analysis corresponds to the *shape feature* of the orthogonal version of the second order derivatives [7] although they are not equal.

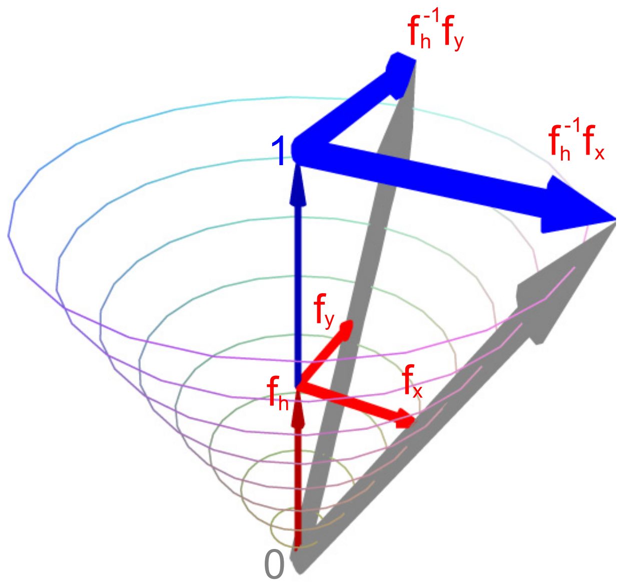

Figure 7.4: Geometric interpretation of the projective space. The underlying 2D space is spanned by the conjugate signal components f_x and f_y and the additional coordinate of the 3D projective space is given by the homogeneous signal component f_h. All i1D and i2D signals can be normalized to a homogenous coordinate 1 by multiplying the components f_x and f_y with f_h^{-1}.

7.4.2 Homogeneous Signal

The geometric interpretation of the mean orientation and the apex angle results from the signal f_s which is embedded in 3D space as a vector $[0, 0, f_s]^T \in \mathbb{R}^3$. This 3D vector will be rotated by the Euler angles $(\alpha, 2\theta_m) \in \left[0, \frac{\pi}{2}\right] \times [0, 2\pi]$ (see figure 7.3).
By means of the apex angle α, a so called homogeneous signal component f_h of the signal f_p in 3D projective subspace of the conformal space will be introduced by

$$f_h := \sqrt{\frac{1 + \cos\alpha}{2}} \in [0, 1] \ .$$

In the following a relation of the signal representation in CGA and the projective space known from computer graphics and computer vision will be shown.

Main Orientation

The local main orientation of the signal can be determined by

$$\theta_m = \arctan \frac{f_h^{-1} f_y}{f_h^{-1} f_x}$$

in projective space. Again, please note that the domain of the main orientation is not equal to the domain of the mean orientation.

7.4.3 Structural Signal Features

The structural signal features are the local phase and the local amplitude.

Phase

The phase of i1D and i2D signals can be evaluated by

$$\phi = \operatorname{atan2}\left(\sqrt{\left[f_h^{-1} f_x\right]^2 + \left[f_h^{-1} f_y\right]^2}, f_p\right)$$

in one unified framework. The phase can be determined by the first order Hilbert transform and the geometric information given by the apex angle which will be delivered by the higher order Hilbert transform.

Amplitude

Also the local amplitude for i1D and i2D signals can be determined by

$$a = \frac{1}{2}\sqrt{f_p^2 + \left[f_h^{-1} f_x\right]^2 + \left[f_h^{-1} f_y\right]^2}$$

in one unified framework. In the case of pure i1D signals the apex angle is zero, i.e. $f_h = 1$. In this case the formulas of the phase and amplitude reduce to those known from the monogenic signal. The advantage of this approach is that it can automatically distinguish between i1D and i2D signals and it can be applied to all kinds of local intrinsic dimension without any previous knowledge about the original signal.
In the case of 2D image signals, this approach is designed for an isotropic analysis of lines, edges, corners and junctions in one framework.
The important generalization from i1D signal analysis to true 2D signal analysis is, that in contrast to the 2D monogenic signal, here the 2D conjugate Poisson components $[f_x, f_y]^T$ are in a natural way located in the higher dimensional 3D projective space $[f_x, f_y, f_h]^T$ with f_h as the additional homogeneous component (see figure 7.4). Signal analysis naturally reduces now to

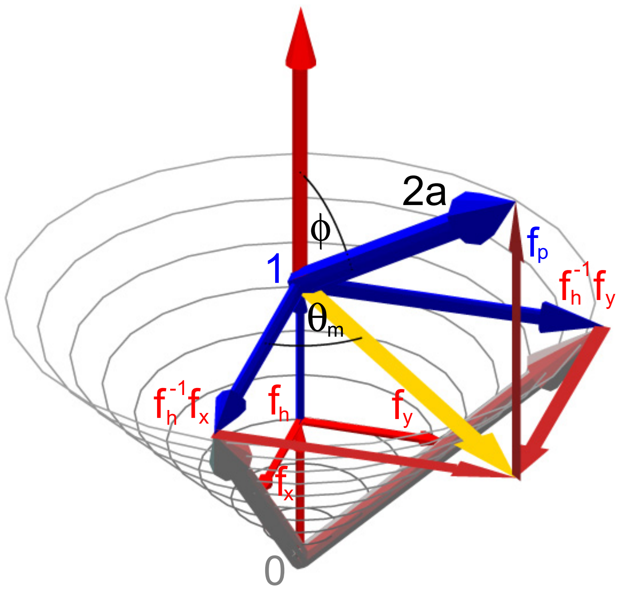

Figure 7.5: Geometric interpretation of phase ϕ, amplitude a and main orientation θ_m in projective space of i1D and i2D signals in one unified framework.

the normalization of the homogeneous component to 1 (see figure 7.6). This can be easily done by multiplying the conjugate Poisson signal components f_x and f_y by f_h^{-1}. In other words: The 2D space spanned by the components f_x and f_y is extended by the homogeneous component f_h which is determined by the geometric information delivered by the apex angle.

7.4.4 Proof

Due to the previous results of the Hilbert transform in Radon space the proofs can now be done by trigonometric calculations using the local signal components

$$
\begin{aligned}
f_p &= 2a\cos\phi \\
f_x &= a\sin\phi\left[\cos\theta_1 + \cos\theta_2\right] \\
f_y &= a\sin\phi\left[\sin\theta_1 + \sin\theta_2\right] \\
f_s &= a\cos\phi \\
f_+ &= a\cos\phi\frac{1}{2}\left[\sin(2\theta_1) + \sin(2\theta_2)\right] \\
f_{+-} &= a\cos\phi\frac{1}{2}\left[\cos(2\theta_1) + \cos(2\theta_2)\right] \ .
\end{aligned}
$$

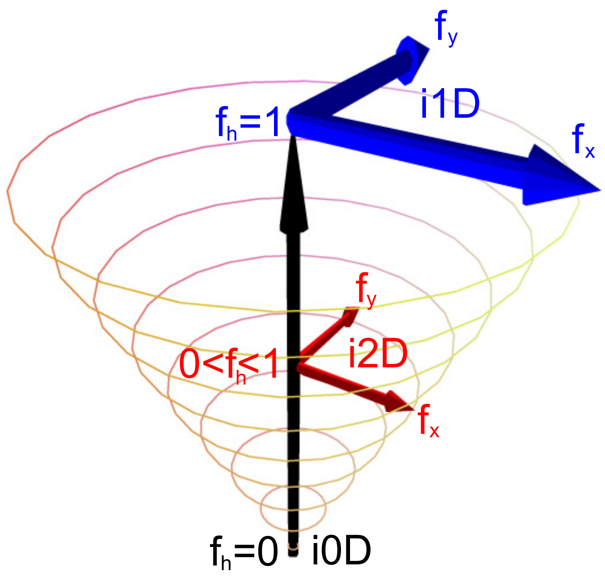

Figure 7.6: This figure illustrates the relation of all intrinsic dimensions and the homogeneous signal component f_h in one continuous space. All i0D signals are located at the focal point $[0,0,0]^T$ of the cone with $f_h = 0$. All i1D signals are located at the 2D subspace with the homogeneous coordinate $f_h = 1$. Any i2D signal is characterized by a homogeneous coordinate $0 < f_h < 1$. Therefore, the i0D signals are on a point of singularity, the i1D signals can be represented by a 2D plane and the i2D signals exist in a 3D volume.

One important result is that the superposition of i1D signals, to model i1D and i2D signals in one framework, corresponds to the extension of the 2D space to the 3D projective space.

Chapter 8

Implementation

The low level phase based analysis approach of 2D signals can be easily integrated into any computer vision software by using the following C++ implementation. Each 2D signal double f(double x,double y) can be locally analyzed at every position (cx,cy) by applying a difference of Poisson (DoP) bandpass filter to the original signal with the fine scale space parameter s_f and the coarse scale space parameter s_c. With the theoretical results of this work it is now possible to analyze the mapping of the original 2D signal to the higher dimensional multivector in conformal space.

```
void AnalyticSignal(double cx,double cy,
                    double& Orientation,double& Phase,
                    double& Amplitude,double& ApexAngle)
{
    double s_c = 0.2; //coarse scale space parameter
    double s_f = 0.1; //fine   scale space parameter
    double dx  = 1;   //convolution step width
    double n   = 5;   //convolution mask size
    double f_p=0,f_x=0,f_y=0,f_xx=0,f_xy=0,f_yy=0;
    //2D convolution
    for (double x = -n;x <= n;x += dx)
    for (double y = -n;y <= n;y += dx)
    {
        double t  = f(x + cx,y + cy)*pow(dx,2);
        double pf = t* Kernel1(x,y,s_f);
        double pc = t* Kernel1(x,y,s_c);
        double k  = t*(Kernel2(x,y,s_f)-Kernel2(x,y,s_c));
        //signal in Poisson scale space
        f_p  += s_f*pf - s_c*pc;
```

```
        //first order Hilbert transform
        f_x  += x   * (pf-pc);
        f_y  += y   * (pf-pc);
        //second order Hilbert transform
        f_xx += x*x * k;
        f_yy += y*y * k;
        f_xy += x*y * k;
    }
    double f_pm   = 0.5*(f_xx-f_yy);
    double f_s    = 0.5* f_p;
    double f_plus = f_xy;
    double e      = sqrt(pow(f_pm,2)+pow(f_plus,2))/fabs(f_s);
    double q      = (pow(f_x,2)+pow(f_y,2)) * 2/(1+e);

    Phase = atan2(sqrt(q),f_p);
    Orientation = ((int)Phase == 0)
                  ? 0.5*atan2(f_plus,f_pm)+M_PI/2
                  : atan2(f_y,f_x);
    Amplitude = 0.5*sqrt(pow(f_p,2)+q);
    ApexAngle = atan2(sqrt(pow(f_s,2)-pow(f_plus,2)-
                pow(f_pm,2)),sqrt(pow(f_plus,2)+pow(f_pm,2)));
}
```

The first order 2D convolution kernels will be calculated by

```
double Kernel1(double x,double y,double s)
{
    double ss = pow(s,2);
    double kk = pow(x,2) + pow(y,2);
    return 1/(2*M_PI*pow(ss + kk,1.5));
}
```

and the second order 2D convolution kernels in spatial domain (x, y) with scale space parameter s will be determined by

```
double Kernel2(double x,double y,double s)
{
    double ss = pow(s,2);
    double kk = pow(x,2) + pow(y,2);
    double d = pow(kk,2) * pow(ss + kk,1.5) * 2*M_PI;
    return (d==0) ? 0 : -(s*(2*ss+3*kk)-2*pow(ss+kk,1.5))/d;
}
```

The time complexity of this algorithm is in $O(n^2)$ with n as the convolution mask size in one dimension. This time complexity can be reduced by calculation in Fourier domain. The disadvantage of the calculation in Fourier domain is the restriction to global signal analysis. By convolution in spatial domain for each position $(x, y) \in \mathbb{R}^2$ an individual scale space parameter can be chosen to enable adaption to the local structural and geometrical information.

Chapter 9

Experimental Results

The 2D analytic signal can be applied to all kinds of 2D signals, e.g. to real and synthetic 2D image signals. In figure 9.1 the results of a pure i1D signal are shown. The synthetic i1D signal is modeled by $f(x, y) := a\cos(x\cos\theta + y\sin\theta + \phi)$ with constant amplitude a, with constant phase ϕ and with constant orientation θ. The resulting local orientation is constant up to $\theta + k\pi$ with $k \in \mathbb{Z}$ since orientation is not uniquely defined in 2D signal domains. The apex angle of the pure i1D signal is zero. The results of the local phase equal the original signal with same amplitude, with same orientation but with by 90° shifted phase.

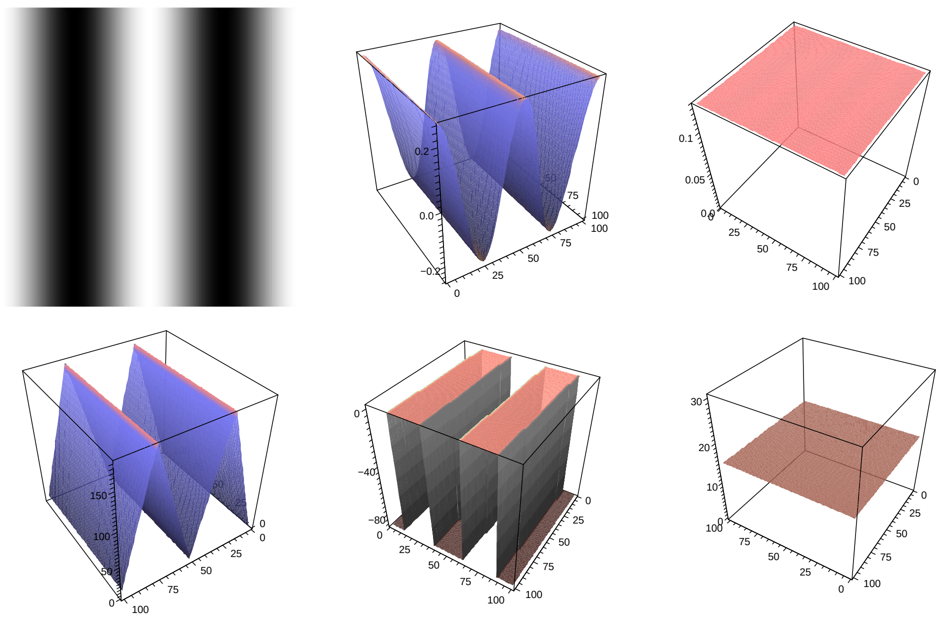

Figure 9.1: Top row from left to right: Pure i1D original signal, original signal in Poisson scale space and local amplitude. Bottom row from left to right: Local phase, orientation and apex angle. Convolution mask size: 7×7 pixels. Scale space parameters: $s_c = 2$ and $s_f = 1$.

In figure 9.2 the results of a pure i2D signal are shown. The synthetic i2D signal is modeled by $f(x,y) := \sum_{i=1}^{2} a\cos(x\cos\theta_i + y\sin\theta_i + \phi)$ with constant amplitude a, with constant phase ϕ and with constant orientations θ_1 and θ_2. The resulting local main orientation is constant up to $\theta + k\pi$ with $k \in \mathbb{Z}$ since orientation is not uniquely defined in 2D signal domains. The apex angle of the pure i2D signal is constant. The results of the local phase depend on the position in spatial domain and the amplitude should be constant.

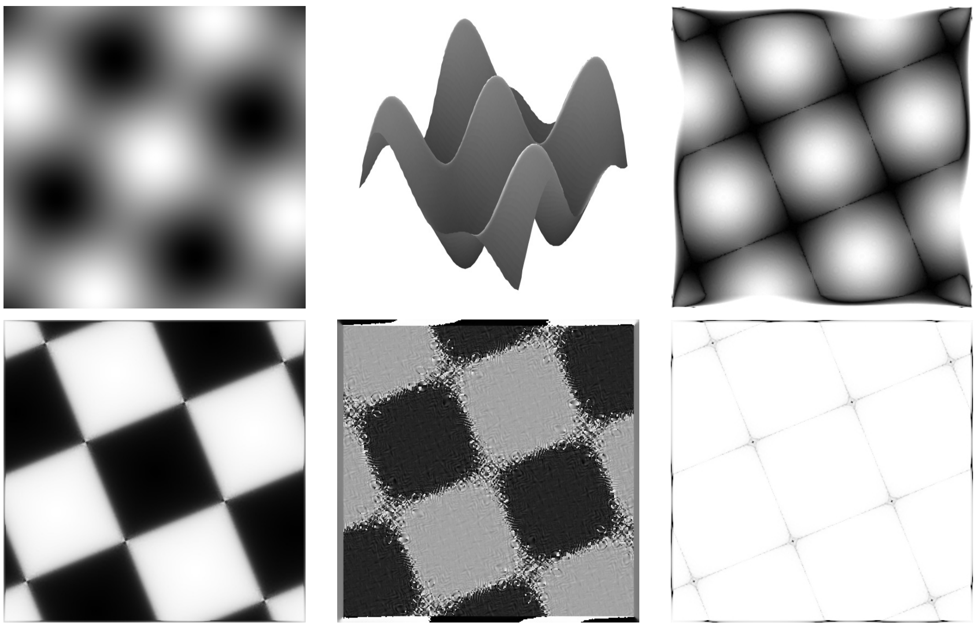

Figure 9.2: Top row from left to right: Pure i2D original signal, original signal in Poisson scale space and local amplitude. Bottom row from left to right: Local phase, orientation and apex angle. Convolution mask size: 7×7 pixels. Scale space parameters: $s_c = 2$ and $s_f = 1$.

Figure 9.3 illustrates the experimental results with known ground truth data (amplitude, phase, orientation and apex angle) of the 2D analytic signal. The estimated features are plotted with fixed orientation and fixed amplitude against varying phase $0 \leqslant \phi \leqslant 180°$ and varying apex angle $0 \leqslant \alpha \leqslant 90°$. Top row left figure: Estimated phase for varying phase and varying apex angle. The phase can be determined exactly. Top row right figure: Estimated amplitude for varying phase and varying apex angle but fixed signal amplitude. Bottom row left figure: Estimated orientation for varying phase and varying apex angle but fixed signal orientation and fixed signal amplitude. The orientation can be determined exactly except for the phase $\phi = 180°$. Bottom row right figure: Estimated apex angle for varying phase and varying apex angle. In figure 9.4 the experimental results of the 2D monogenic signal [11] applied to i1D and i2D signals with constant orientation and constant amplitude are shown. Top row left figure: Estimated phase against varying phase and varying apex angle. The errors increase with increasing apex angle. In the ideal case the result should look like the plane in figure 9.3. Top row right figure: Estimated amplitude against varying phase and varying apex angle. The amplitude should be constant like in

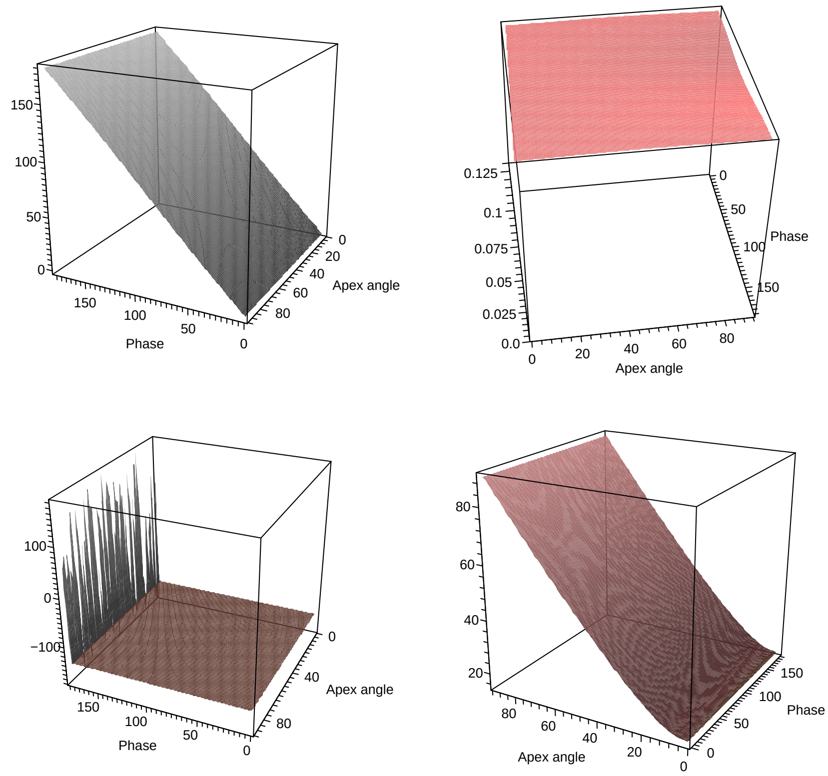

Figure 9.3: Top row from left to right: Local phase and amplitude. Bottom row from left to right: Orientation and apex angle. Convolution mask size in spatial domain: 7×7 pixels. Coarse scale space parameter: $s_c = 0.2$, and fine scale space parameter: $s_f = 0.1$.

figure 9.3. Bottom row left figure: Estimated orientation against varying phase and varying apex angle. The orientation can be determined exactly except for the phases $\phi = 0°$ and $\phi = 180°$. The results show that in contrast to the 2D analytic signal in figure 9.3 the amplitude and phase of the 2D monogenic signal produce significant errors. It is important to mention that the 2D analytic signal performs also in case of i1D signals better than the 2D monogenic signal since finite signals are never of intrinsic dimension one.

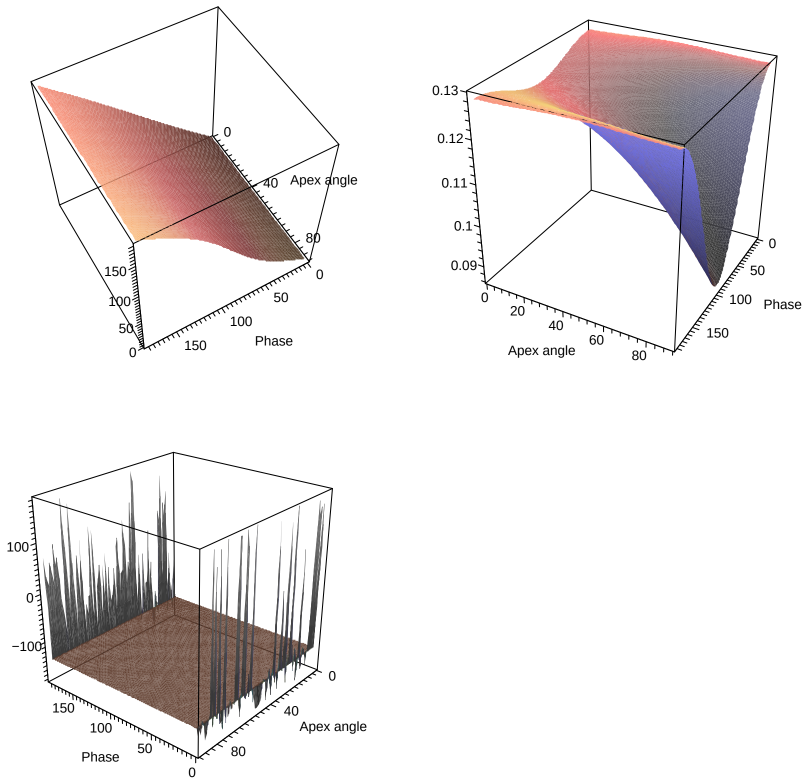

Figure 9.4: Top row from left to right: Local i1D phase and amplitude. Bottom row: Local orientation. Convolution mask size in spatial domain: 7×7 pixels. Coarse scale space parameter: $s_c = 0.2$, and fine scale space parameter: $s_f = 0.1$.

Chapter 10

Generalization of the 2D Analytic Signal

According to [28] a general mapping from $T \in M(2, \langle \mathbb{R}_3 \rangle_2)$ to $\varphi(T) \in \mathbb{R}_{4,1}$ with $\langle \cdot \rangle_n$ as the grade n projection can be defined. Now, also tensor like matrices can be easily mapped to the geometric algebra of the conformal space (CGA). With the basis vectors $\{1, \mathbf{i}, \mathbf{j}, \mathbf{k}\}$ of the quaternions $\mathbb{H}$ and the isomorphism $\mathbf{i} \cong \mathbf{e}_{12}$, $\mathbf{j} \cong \mathbf{e}_{23}$ and $\mathbf{k} \cong \mathbf{e}_{31}$ a hypercomplex or Clifford valued matrix can be defined by the Hilbert transform of second order (with T^e as the even part) and the Hilbert transform of third order (with T^o_x and T^o_y as the odd parts) (this has been proposed in tensor form by [30])

$$T := \underbrace{\begin{bmatrix} f_{xx} & f_{xy} \\ f_{xy} & f_{yy} \end{bmatrix}}_{T^e} \mathbf{i} + \underbrace{\begin{bmatrix} f_{xxx} & f_{xxy} \\ f_{xxy} & f_{xyy} \end{bmatrix}}_{T^o_x} \mathbf{j} + \underbrace{\begin{bmatrix} f_{xxy} & f_{xyy} \\ f_{xyy} & f_{yyy} \end{bmatrix}}_{T^o_y} \mathbf{k}$$

which will be mapped to a multivector of the CGA by

$$\begin{aligned} \varphi(T) &= \frac{1}{2}\left[f_p \mathbf{i} + f_x \mathbf{j} + f_y \mathbf{k}\right] \\ &+ \left[f_{xy} \mathbf{i} + f_{xxy} \mathbf{j} + f_{xyy} \mathbf{k}\right] \mathbf{e}_{+} \\ &+ \frac{1}{2}\left[f^{-} \mathbf{i} + f^{-}_x \mathbf{j} + f^{-}_y \mathbf{k}\right] \mathbf{e}_{+-} \end{aligned}$$

with the signal components

$$\begin{aligned} f_p &:= f_{xx} + f_{yy} \\ f_x &:= f_{xxx} + f_{xyy} \\ f_y &:= f_{xxy} + f_{yyy} \\ f^- &:= f_{xx} - f_{yy} \\ f_x^- &:= f_{xxx} - f_{xyy} \\ f_y^- &:= f_{xxy} - f_{yyy} \, . \end{aligned}$$

Note, that up to now we did not exploit the whole information given by this multivector in conformal space. The unused signal components of the third order Hilbert transform are: f_x^- and f_y^-. These so far unused components have to be used for the generalization of the 2D analytic signal.
The goal of this work is the most general formulation of the *2D analytic signal*. Up to now the first and second order Hilbert transforms have been sufficient for signal analysis. We will now take advantage of the general isomorphism $\varphi(T)$ which maps the set of 2×2 - Clifford valued matrices to the set of multivectors in conformal space. Therefore also the third order Hilbert transform can be used for 2D signal analysis.
Without loss of generality the assumed combined i1D / i2D signal model in scale space reads

$$\mathcal{P}\{f\}(x, y; s) = \sum_{i=1}^{2} a_i \cos(x \cos\theta_i + y \sin\theta_i + \phi_i)$$

(arguments for this signal model have been given by [10]) with the unknown local amplitudes a_1 and a_2, the unknown local orientations θ_1 and θ_2, the unknown local phases ϕ_1 and ϕ_2, the Poisson filtered signal f_p, the known results of the first order Hilbert transforms $[f_x, f_y]^T$ and the known second order Hilbert transforms $[f_{xx}, f_{xy}, f_{yy}]^T$.
The local signal model at the origin $(x, y) := (0, 0)$ of the applied local coordinate system results in

$$f_p = \sum_{i=1}^{2} a_i \cos\phi_i = \mathcal{P}\{f\}(0, 0; s)$$

with $f_i^e := a_i \cos\phi_i$ as the even parts. By means of the Radon space interpretation the first order Hilbert transform results in

$$\begin{bmatrix} f_x \\ f_y \end{bmatrix} = \sum_{i=1}^{2} a_i \sin\phi_i \begin{bmatrix} \cos\theta_i \\ \sin\theta_i \end{bmatrix}$$

with $f_i^o := a_i \sin\phi_i$ as the odd parts. This system of linear equations can be solved for the odd parts by using the Cramer's rule

$$\begin{bmatrix} f_1^o \\ f_2^o \end{bmatrix} = \frac{1}{\sin(\theta_1 - \theta_2)} \begin{bmatrix} f_y \cos\theta_2 - f_x \sin\theta_2 \\ f_x \sin\theta_1 - f_y \cos\theta_1 \end{bmatrix} .$$

Same with the following system of linear equations

$$\begin{bmatrix} f_p \\ f_{xy} \end{bmatrix} = \sum_{i=1}^{2} f_i^e \begin{bmatrix} 1 \\ \sin\theta_i \cos\theta_i \end{bmatrix}$$

which can be solved for the even parts

$$\begin{bmatrix} f_1^e \\ f_2^e \end{bmatrix} = \frac{1}{\cos(\theta_1 + \theta_2)\sin(\theta_1 - \theta_2)} \begin{bmatrix} \frac{f_p}{2}\sin(2\theta_2) - f_{xy} \\ f_{xy} - \frac{f_p}{2}\sin(2\theta_1) \end{bmatrix} .$$

Now the systems of linear equations can be solved for the two unknown phases by the following ansatz

$$\begin{aligned} \phi_1 &= \arctan\frac{f_1^o}{f_1^e} = \arctan\left(\cos(\theta_1+\theta_2)\frac{f_y\cos\theta_2 - f_x\sin\theta_2}{\frac{f_p}{2}\sin(2\theta_2) - f_{xy}}\right) \\ \phi_2 &= \arctan\frac{f_2^o}{f_2^e} = \arctan\left(\cos(\theta_1+\theta_2)\frac{f_x\sin\theta_1 - f_y\cos\theta_1}{f_{xy} - \frac{f_p}{2}\sin(2\theta_1)}\right) . \end{aligned}$$

The two unknown amplitudes can be derived by

$$a_i = \sqrt{[f_i^e]^2 + [f_i^o]^2}, \quad i \in \{1, 2\} .$$

Hence, the given inverse problem has been reduced to the search for the orientations θ_1 and θ_2.
The system of linear equations resulting from the Radon interpretation of the second order Hilbert transform reads

$$\begin{bmatrix} f_{xx} \\ f_{xy} \\ f_{yy} \end{bmatrix} = \sum_{i=1}^{2} f_i^e \begin{bmatrix} \cos^2\theta_i \\ \sin\theta_i\cos\theta_i \\ \sin^2\theta_i \end{bmatrix} .$$

Plugging in the solution for the even parts f_i^e for $i \in \{1, 2\}$ in

$$f^- := f_{xx} - f_{yy} = \sum_{i=1}^{2} f_i^e \cos(2\theta_i)$$

yields the equation

$$\begin{aligned}
&\cos(\theta_1+\theta_2)\sin(\theta_1-\theta_2)f^- \\
&= \cos(2\theta_1)\left[\frac{f_p}{2}\sin(2\theta_2)-f_{xy}\right]+\cos(2\theta_2)\left[f_{xy}-\frac{f_p}{2}\sin(2\theta_1)\right]
\end{aligned}$$

and results in

$$\begin{aligned}
&\left[\frac{f^-}{2}\sin(2\theta_1)-f_{xy}\cos(2\theta_1)+\cos(2\theta_2)\left[f_{xy}-\frac{f_p}{2}\sin(2\theta_1)\right]\right]^2 \\
&= \left[1-\cos^2(2\theta_2)\right]\left[\frac{f^-}{2}-\frac{f_p}{2}\cos(2\theta_1)\right]^2
\end{aligned}$$

which must be solved for $\cos(2\theta_2)$.
The next step is to use the third order Hilbert transform $[f_{xxx}, f_{xxy}, f_{xyy}, f_{yyy}]^T$ to solve for $\cos(2\theta_2)$. The last step will be the solution for both orientations so that the whole system of equations can be solved.
The third order Hilbert transform results in

$$\begin{bmatrix} f_{xxx} \\ f_{xxy} \\ f_{xyy} \\ f_{yyy} \end{bmatrix} = \sum_{i=1}^{2} f_i^o \begin{bmatrix} \cos^3\theta_i \\ \cos^2\theta_i\sin\theta_i \\ \cos\theta_i\sin^2\theta_i \\ \sin^3\theta_i \end{bmatrix}$$

with $f_x^- := f_{xxx} - f_{xyy}$ and $f_y^- := f_{xxy} - f_{yyy}$.
Plugging in the odd parts f_i^o for $i \in \{1,2\}$ results in

$$\begin{aligned}
&\sin(\theta_1-\theta_2)f_x^- = \\
&\cos\theta_1\cos(2\theta_1)\left[f_y\cos\theta_2-f_x\sin\theta_2\right]+\cos\theta_2\cos(2\theta_2)\left[f_x\sin\theta_1-f_y\cos\theta_1\right]
\end{aligned}$$

and

$$\begin{aligned}
&\sin(\theta_1-\theta_2)f_y^- = \\
&\sin\theta_1\cos(2\theta_1)\left[f_y\cos\theta_2-f_x\sin\theta_2\right]+\sin\theta_2\cos(2\theta_2)\left[f_x\sin\theta_1-f_y\cos\theta_1\right]
\end{aligned}$$

which can be solved for either θ_1 or θ_2. The solution reads

$$\cos(2\theta_2) = \frac{f_x^-\sin\theta_1 - f_y^-\cos\theta_1}{f_x\sin\theta_1 - f_y\cos\theta_1}\ .$$

The next step will be the solution for θ_1.
After that the last step will be the search for the geometric interpretation using geometric algebra.

It has been shown that the search for the generalization to the 2D analytic signal can be solved by a divide and conquer approach which splits the analysis in one geometric part which consists of the orientations and the apex angles and a second structural part which consists of the amplitudes and phases. If the geometric information can be determined, the amplitudes and phases can be also determined.

Chapter 11

Conclusion

In this report a novel generalization of the monogenic signal to the 2D analytic signal has been presented. Both i1D and i2D signals such as edges, lines, corners and junctions can be exactly analyzed in a rotationally invariant way without steering in one unified algebraic framework - called the hybrid matrix geometric algebra. Our approach degenerates to the 2D monogenic signal for the case of i1D signals. Local signal features such as amplitude, phase, apex angle and orientation are orthogonal components (split of identity) in monogenic scale space. The approach can be easily implemented into existing computer vision applications by convolution with five 2D kernels in spatial domain. We presented a further step in the evolution process of the analytic signal which maps a real signal to a complex valued signal and the 2D monogenic signal which maps a real signal to a vector valued signal in Euclidean space. This approach maps a real 2D signal to a multivector valued signal in conformal space which can be geometrically interpreted in a descriptive way in a projective subspace of the conformal space.
We also gave a constructive outlook for the generalization of the 2D analytic signal to all kinds of 2D signal models.

Acknowledgements

This work was supported by the German Research Foundation (DFG) under the project *SO-320/4-2* (Gerald Sommer).

Bibliography

[1] S. Bernstein. Inverse Probleme. Technical report, TU Bergakademie Freiberg, 2007.

[2] J. Beyerer and F. P. Leon. The Radon transform in digital image processing. *Automatisierungstechnik*, 50(10):472–480, 2002.

[3] R. N. Bracewell. *Fourier Analysis and Imaging*. Kluwer Academic Plenum Publishers, 2003.

[4] F. Brackx, B. De Knock, and H. De Schepper. Generalized multidimensional Hilbert transforms in Clifford analysis. *International Journal of Mathematics and Mathematical Sciences*, 2006.

[5] T. Bülow and G. Sommer. Hypercomplex signals - a novel extension of the analytic signal to the multidimensional case. *IEEE Transactions on Signal Processing*, 49(11):2844–2852, 2001.

[6] G. Carneiro and A. D. Jepson. Phase-based local features. In *7th European Conference on Computer Vision-Part I*, volume 2350 of *LNCS*, pages 282–296. Springer-Verlag, Berlin, Heidelberg, New York, 2002.

[7] P. E. Danielsson, Q. Lin, and Q. Z. Ye. Efficient detection of second-degree variations in 2D and 3D images. *Journal of Visual Communication and Image Representation*, 12(3):255–305, 2001.

[8] R. Delanghe. Clifford analysis: History and perspective. *Computational Methods and Function Theory*, 1(1):107–153, 2001.

[9] M. P. do Carmo. *Differential Geometry of Curves and Surfaces*. Prentice-Hall, 1976.

[10] M. Felsberg. Low-level image processing with the structure multivector. Technical Report 2016, Kiel University, Department of Computer Science, 2002.

[11] M. Felsberg and G. Sommer. The monogenic signal. *IEEE Transactions on Signal Processing*, 49(12):3136–3144, 2001.

[12] M. Felsberg and G. Sommer. The monogenic scale-space: A unifying approach to phase-based image processing in scale-space. *Journal of Mathematical Imaging and Vision*, 21:5–26, 2004.

[13] D. J. Fleet and A. D. Jepson. Stability of phase information. *IEEE Transactions on Pattern Analysis and Machine Intelligence*, 15(12):1253–1268, 1993.

[14] D. J. Fleet, A. D. Jepson, and M. R. M. Jenkin. Phase-based disparity measurement. *CVGIP: Image Understanding*, 53, 1991.

[15] O. Fleischmann. 2D Clifford Signal Analysis. Master's thesis, Department of Computer Science, Kiel University, Germany, 2008.

[16] D. Gabor. Theory of communication. *Journal IEE, London*, 93(26):429–457, 1946.

[17] I. S. Gradshteyn and I. M. Ryzhik. *Table of Integrals, Series, and Products.* Academic Press Elsevier, Amsterdam, Boston, Heidelberg, London, New York, Oxford, Paris, San Diego, San Francisco, Singapore, Sydney, Tokio, 2007.

[18] G. H. Granlund and H. Knutsson. *Signal Processing for Computer Vision.* Kluwer Academic Publisher, Dordrecht, 1995.

[19] S. L. Hahn. *Hilbert Transforms in Signal Processing.* Artech House Inc, Boston, London, 1996.

[20] T. Huang, J. Burnett, and A. Deczky. The importance of phase in image processing filters. *IEEE Trans. on Acoustics, Speech and Signal Processing*, 23(6):529–542, 1975.

[21] T. Iwaniec and G. Martin. *Geometric Function Theory and Non-linear Analysis.* Oxford University Press, USA, 2002.

[22] B. Jähne. *Digital Image Processing.* Springer, 2001.

[23] A. Markoe. *Analytic Tomography.* Cambridge University Press, Cambridge, 2006.

[24] A. V. Oppenheim and J. S. Lim. The importance of phase in signals. *Proceedings of the IEEE*, 69(5):529–541, 1981.

[25] C. B. U. Perwass and D. Hildenbrand. Aspects of geometric algebra in euclidean, projective and conformal space. Technical Report 0310, Kiel University, Department of Computer Science, 2003.

[26] B. Rieger and L. J. van Vliet. Representing orientation in n-dimensional spaces. In *CAIP*, volume 2756 of *LNCS*, pages 17–24. Springer-Verlag, Berlin, Heidelberg, New York, 2003.

[27] B. Rosenhahn and G. Sommer. Pose estimation in conformal geometric algebra part one: The stratification of mathematical spaces. *Journal of Mathematical Imaging and Vision*, 22(1):27–48, 2005.

[28] G. Sobczyk and G. Erlebacher. Hybrid matrix geometric algebra. In H. Li, P. J. Olver, and G. Sommer, editors, *Computer Algebra and Geometric Algebra with Applications*, volume 3519 of *LNCS*, pages 191–206. Springer-Verlag, Berlin, Heidelberg, New York, 2005.

[29] Z. Xiaoxun and J. Yunde. Local steerable phase (lsp) feature for face representation and recognition. In *CVPR '06: Proceedings of the 2006 IEEE Computer Society Conference on Computer Vision and Pattern Recognition*, pages 1363–1368. IEEE Computer Society, 2006.

[30] D. Zang and G. Sommer. Signal modeling for two-dimensional image structures. *Journal of Visual Communication and Image Representation*, 18(1):81–99, 2007.

[31] C. Zetzsche and E. Barth. Fundamental limits of linear filters in the visual processing of two-dimensional signals. *Vision Research*, 30:1111–1117, 1990.